COGNITIVE NEUROSCIENCE

Gut microbial-derived indole-3-propionate improves cognitive function in Alzheimer's disease

Ling Li[1]†, Mengzhen Jia[1]†, Cong Yang[1]†, Yihang Zhao[1], Jun Hu[2], Yu Zhao[1], Xinyu Hu[1], Fangjie Ning[1], Chen Ding[1], Qingyuan Li[1], Jun Gong[1], Xiaoran Jia[1], Kun Xu[3], Yuhao Wang[1], Shuang Zhou[1], Lu Deng[3], Lin Shi[4], Xuhui Chen[2]*, Xuebo Liu[1]*, Zhigang Liu[1,3,5]*

Intermittent fasting (IF) offers a potential strategy to counteract Alzheimer's disease (AD) progression. In our 16-week study on AD transgenic mice, IF positively affected cognitive function and reduced amyloid-β (Aβ) accumulation, verifying the IF's role in modulating neuroinflammation. Multiomics integration revealed strong links between IF-induced hippocampal gene expression, gut microbiota, and serum metabolites beneficial for cognition. Indole-3-propionic acid (IPA) emerged as a pivotal microbial metabolite. Blocking its neuronal receptor, pregnane X receptor (PXR), abolished IF's effects. Human data paralleled these findings, showing lower IPA levels in patients with mild cognitive impairment and AD than in controls. IPA supplementation and IPA-producing *Clostridium sporogenes* reproduced IF's cognitive benefits, whereas PXR blockade in neurons or disruption of IPA synthesis abrogated them. IPA crossed the blood-brain barrier, exhibited potent anti-inflammatory activity, and suppressed Aβ accumulation, essential for neuroprotection. These results underscore microbial metabolites regulated by IF, particularly IPA, as therapeutic candidates for AD, highlighting the critical role of the gut-brain axis in neurodegeneration.

INTRODUCTION

Alzheimer's disease (AD), affecting 43 million people worldwide, is a leading neurodegenerative disease causing dementia (*1*). AD is characterized by cognitive impairment resulting from the accumulation of amyloid-β (Aβ) peptides and intracellular neurofibrillary tangles caused by hyperphosphorylated Tau protein in the brain (*1*, *2*). In addition, AD leads to synaptic damage and neuroinflammation in the brain (*3*). However, the precise etiological mechanisms underlying AD remain unclear. There is an urgent need for effective medical treatments and nonpharmacological nutritional interventions to prevent the development of AD. The risk of AD is associated with nongenetic factors, such as obesity, lack of physical exercise, and an unhealthy diet (*4*).

Over the past few decades, the benefits of dietary restriction for brain health and dementia prevention have been widely documented (*5*). Likewise, intermittent fasting (IF) has shown promising effects on metabolic syndrome and cognitive impairment (*6*). Specifically, IF has been shown to improve cognitive function in elderly individuals through biochemical and metabolic changes over a 36-month follow-up period (*7*). Animal studies have suggested that IF may alleviate memory deficits by increasing the expression of neurotrophic factors, enhancing synaptic plasticity, and inhibiting neuroinflammatory responses (*8*–*11*). A recent study showed that a 3-month IF regimen enhanced spatial cognition and hippocampal neurogenesis in female mice (*12*). Notably, IF has been found to reduce Aβ accumulation—a key indicator of AD development—and to prevent memory loss in ovariectomized rats infused with Aβ (*13*, *14*). The neuroprotective mechanism of IF may be linked to its anti-inflammatory and antioxidant effects, the improvement of hippocampal synaptic plasticity, and increased activity of neurotrophic factors, although these remain elusive (*10*, *15*). A recent study indicates that IF could prevent cognitive decline in AD model mice by regulating gut microbiota and amino acid metabolism (*16*). It has also been reported that time-restricted feeding improves memory in AD mice by ameliorating the misalignment of circadian rhythmicity (*17*).

The gut microbiome modulates host brain function, including cognitive behavior, via the gut-brain axis (*18*). Studies have found that gut microbiota composition is altered in patients with AD (*19*, *20*) and that transplantation of fecal microbiota from patients with AD to rats could lead to loss of hippocampal neurogenesis and behavioral impairment (*21*). Our previous study demonstrated that IF prevented synaptic structure damage and cognitive decline in mice with type 2 diabetes. This prevention was attributed to enhanced mitochondrial biogenesis and energy metabolism gene expression in the hippocampus, reshaping the gut microbiome and elevating the levels of beneficial microbial metabolites, such as short-chain fatty acids and the tryptophan microbial metabolite 3-indolepropionic acid (IPA) (*9*). IPA has been widely reported to have neuroprotective effects, including preventing toxicity of Aβ, enhancing nerve regeneration after constriction injury, protecting blood-brain barrier (BBB) function, and anti-neuroinflammation (*22*–*25*). However, studies aiming to explore whether IF-induced alterations in the gut microbiome and microbial metabolites, especially IPA, could prevent cognitive deficits in AD are unexpectedly lacking.

In this study, the transgenic AD models, including Aβ precursor protein (APP)swe/PSEN1dE9(PS1) and 5×FAD mice, were used to investigate the effects of IF on alleviating cognitive deficits in AD. Integrative modeling of the hippocampal transcriptome, gut microbiome, and metabolome was conducted to uncover the biological mechanisms underlying the observed benefits of IF in alleviating cognitive impairments. Furthermore, we explored the role played by IPA in mediating IF's neuroprotective effects on AD. Our findings

[1]College of Food Science and Engineering, Northwest A&F University, Yangling 712100, China. [2]Peking University Shenzhen Hospital, Shenzhen, Guangdong 518004, China. [3]College of Animal Science and Technology, Northwest A&F University, Yangling 712100, China. [4]College of Food Engineering and Nutritional Science, Shaanxi Normal University, Xi'an 710119, China. [5]Northwest A&F University Shenzhen Research Institute, Shenzhen, Guangdong 518000, China.
*Corresponding author. Email: zhigangliu@nwsuaf.edu.cn (Z.L.); xueboliu@nwsuaf.edu.cn (X.L.); xuhuichen@pkuszh.com (X.C.)
†These authors contributed equally to this work.

suggest that IF is a potential dietary restriction strategy for preventing AD development by regulating gut microbiota composition and enhancing IPA generation, which in turn reduces Aβ accumulation and neuroinflammation, consequently preserving cognitive function.

RESULTS

IF alleviates cognitive impairment and Aβ deposition in a mouse model of AD

Four-month-old male and female APP/PS1 transgenic mice (AD model) and their wild-type (WT) littermates were subjected to either ad libitum feeding or an IF regimen (24-hour cycles) for 16 weeks (Fig. 1A). We recorded the weight of mice in each group on the fasting day (fig. S1A). IF reduced body weight gain and food intake while increasing water intake in both genotypes of mice (Fig. 1, B and C, and fig. S1B).

The effect of IF on cognitive function was assessed using the Morris water maze test. Compared with the WT mice, the AD mice had a longer escape latency on navigation tests, indicating that they were cognitively impaired (Fig. 1D). IF decreased the escape latency in the day 6 navigation test, which indicated that IF improved cognition of the AD mice (Fig. 1D). As shown in fig. S1C, the trajectory of mice on the probe day was also recorded. The accumulation of Aβ plaques in the brains of AD mice was measured by immunofluorescence staining (Fig. 1E). IF might reduce the Aβ plaque deposition in the piriform cortex of the AD mouse brain (Fig. 1, E and F), accompanied with a notable decrease gene expression of *Bace-1*, a key enzyme associated with Aβ production. The pathological features of AD are related to abnormal synaptic plasticity, which can be affected by the accumulation of Aβ plaques (*26*).

IF improves synapse ultrastructure and alters hippocampal gene expression

Postsynaptic density (PSD) is a complex subcellular domain that forms an essential protein network and modulates synaptic plasticity (*27*). In AD mice, both the PSD length and width were reduced compared to those in WT mice (Fig. 1G). However, IF increased the length and width of the PSD in the AD mouse hippocampus (Fig. 1, H and I). Consistently, IF up-regulated the mRNA expression of *PSD-95*, a critical gene regulating PSD structure, in the hippocampus of AD mice (fig. S1G).

Moreover, IF reduced ionized calcium binding adaptor molecule 1 (IBA-1) expression, a marker of microglial activation, in the piriform cortex and CA1 regions of AD mice (fig. S1, E and F). Similarly, IF down-regulated the expression of *APP*, *Bace-1*, and *TNF*α while up-regulating the anti-inflammatory cytokine *IL-10* in the hippocampus of AD mice (fig. S1, D and H to J).

Furthermore, we performed RNA sequencing with mouse hippocampi to identify key biological processes and pathways that might be altered by IF. A total of 56,090 genes was detected, including 14,100 newly predicted genes lacking annotation. We found that 1709, 1559, and 1090 genes were differentially expressed in the hippocampus in AD mice, WT mice, and mice in a combined group that contained both AD and WT mice without considering genotype after IF [analysis of variance (ANOVA), $P < 0.05$]. Significant discrepancies were noted among the gene panels when comparing AD + ad libitum to AD + IF, WT + ad libitum to WT + IF, and ad libitum to IF, regardless of genotype (fig. S1K). This discrepancy suggested a gene type effect on hippocampal response to IF regimen.

We focused on genes that were up- ($n = 1103$) or down-regulated ($n = 606$) by IF in AD mice ($P < 0.05$). Compared to ad libitum feeding, IF resulted in differential expression of AD mouse genes that were associated with 280 Kyoto Encyclopedia of Genes and Genomes (KEGG) pathways (table S1). Genes that were highly expressed after IF were enriched in wingless-related integration site signaling, mammalian target of rapamycin signaling, autophagy, hippo signaling, Notch signaling, mitogen-activated protein kinase signaling, and sphingolipid signaling ($P < 0.05$). Genes down-regulated by IF were enriched in pathways related to primary bile acid and unsaturated fatty acid biosynthesis ($P < 0.05$). Particular focus was given to 175 differentially expressed genes in AD + ad libitum versus AD + IF mice that are proposed to be involved in pathways related to AD physiology, oxidative phosphorylation, neurotrophin signaling pathway, and synapse (Fig. 1J and table S2). We observed a clear discrimination between AD + ad libitum versus AD + IF (fig. S1L). Expression of *Gadd45b*, *Zfyve1*, *Ap3d1*, *Cpt1c*, *Lamp2*, and *Foxo6* in AD mouse hippocampi was greatly enhanced by IF (Fig. 1K; Student's *t* test, $P < 0.05$); expression levels were confirmed by quantitative polymerase chain reaction (qPCR) analysis (fig. S1M). Therefore, IF could alleviate cognitive dysfunction in AD mice by reducing Aβ accumulation, accompanied by improved synaptic structure and down-regulated neuroinflammation.

IF reshapes the gut microbiome and metabolome in AD mice

The gut microbiome has vital functions in AD physiology (*28*). We analyzed gut microbiota composition in mouse fecal samples using 16*S* ribosomal RNA (rRNA) v3-v4 gene amplicon sequencing. IF did not significantly affect α or β diversity of gut microbiota within the ad libitum group (fig. S2A). However, α and β diversity differed significantly between ad libitum and IF groups in terms of microbial genera and operational taxonomic units (OTUs; fig. S2B). Specifically, we identified optimal bacterial panels at the genus and OTU levels to distinguish between ad libitum and IF groups, with or without considering the genotype. The panels were derived by using partial least squares discriminant analysis (PLS-DA) incorporated into a repeated double cross-validation framework with an all-relevant variable selection procedure. Compared with the ad libitum group, IF altered the abundance of 181 bacterial species in WT mice, as well as the abundance of 250 bacterial species in AD mice (fig. S2B). There is a distinct separation between the ad libitum and IF treatment (fig. S2C). Most of the differential bacterial species were included in the multivariate models distinguishing WT + ad libitum from WT + IF, as well as ad libitum from IF groups across both AD and WT mice. This result indicated the robustness of IF-induced changes in the abundance of bacteria. Individually, IF significantly altered the relative abundance of 28 OTUs in AD mice (Fig. 2A). Compared with AD mice, IF greatly promoted the growth of *Lactobacillus* and several OTUs belonging to *Lactobacillus*, whereas it led to a lower relative abundance of *Turicibacter* and *Yaniella* (Fig. 2B and fig. S2D). Phylogenetic investigation of communities by reconstruction of unobserved states (PICRUSt) analysis revealed that IF up-regulated genes enriched in pathways related to apoptosis, primary and secondary bile acid metabolism, and fatty acid biosynthesis compared with the ad libitum group of AD mice (table S3).

IF greatly affected the plasma metabolome, and notably, a gene type–specific effect on IF-induced changes in plasma metabolites was observed. Specifically, 348 and 182 metabolites were optimally selected as key metabolites relevant to IF in the AD and WT groups,

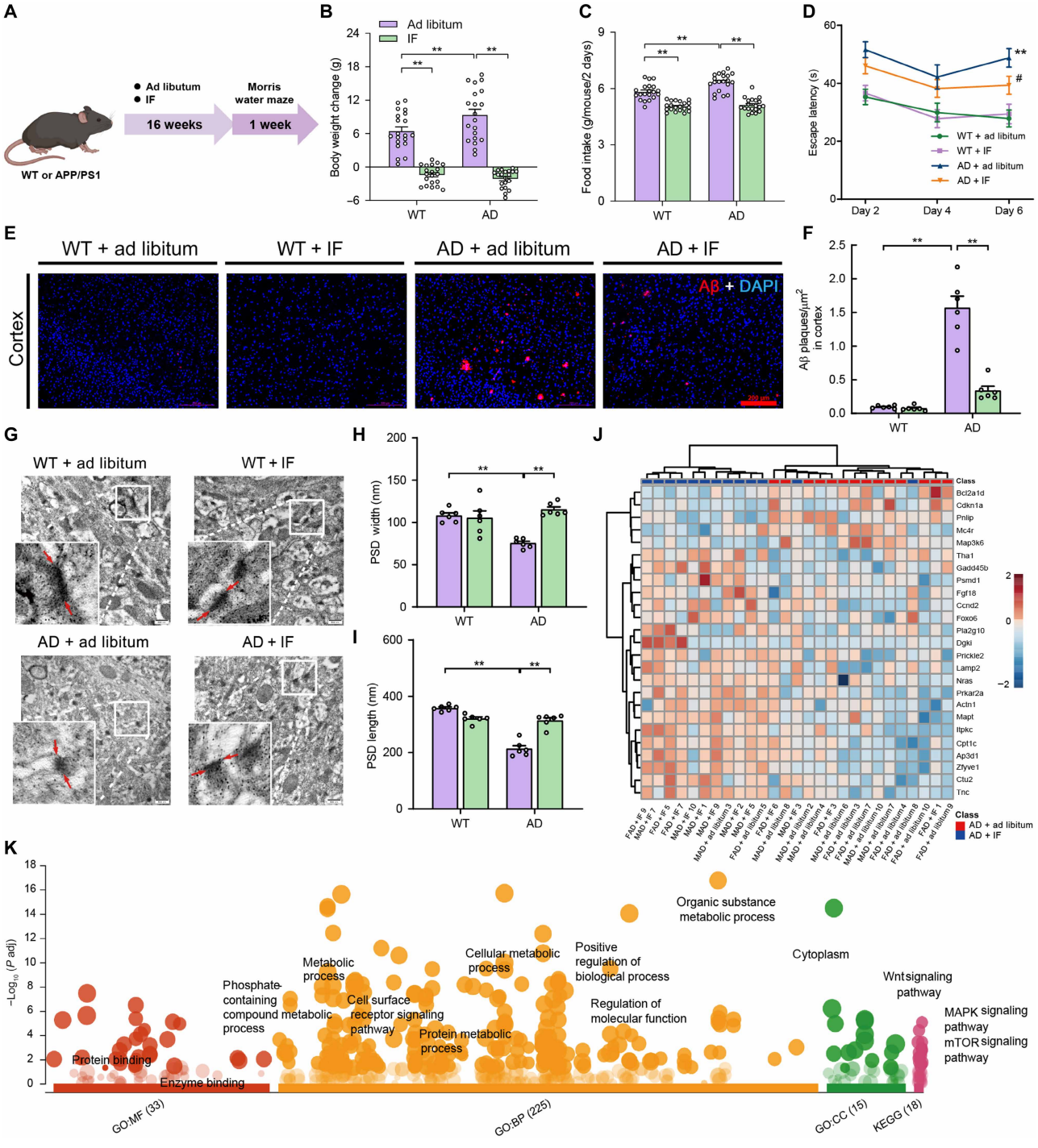

Fig. 1. IF alleviates cognitive impairment and Aβ deposition and protects the synapse ultrastructure in AD mice. (**A**) Schematic of the treatment with IF or ad libitum in each group (WT + ad libitum: $n = 20$, WT + IF: $n = 20$, AD + ad libitum: $n = 20$, AD + IF: $n = 20$). (**B**) Body weight change ($n = 20$). (**C**) Food intake ($n = 20$). (**D**) Escape latency ($n = 20$). Cognitive function was measured by the Morris water maze test (see Materials and Methods). (**E**) Representative immunofluorescence images of Aβ plaques in the piriform cortex ($n = 6$ slices per group). Scale bars, 200 μm. (**F**) Aβ plaque density (number of plaques per square micrometer) in the piriform cortex ($n = 6$). (**G**) Representative images of the ultrastructure of synapse in the hippocampus of female mice ($n = 6$). (**H** and **I**) The length and width of PSD in the hippocampus of mice ($n = 6$). (**J**) A *z*-score scaled heatmap of 175 differentially expressed genes between AD + ad libitum and AD + IF with $P < 0.05$. The top 25 genes are presented. (**K**) Gene Ontology (GO) and KEGG pathway annotations for 175 genes whose expression differed between AD + ad libitum and AD + IF. Wnt, wingless-related integration site; mTOR, mammalian target of rapamycin; MAPK, mitogen-activated protein kinase. In (D), * indicates a significant difference between WT + ad libitum and AD + ad libitum, while # indicates a significant difference between AD + ad libitum and AD + IF. Data are mean ± SEM. $^{**}P < 0.01$ and $^{\#}P < 0.05$. Significant differences between means were determined by two-way ANOVA with Tukey's multiple comparisons test. DAPI, 4′,6-diamidino-2-phenylindole; mTOR, mammalian target of rapamycin; MAPK, mitogen-activated protein kinase.

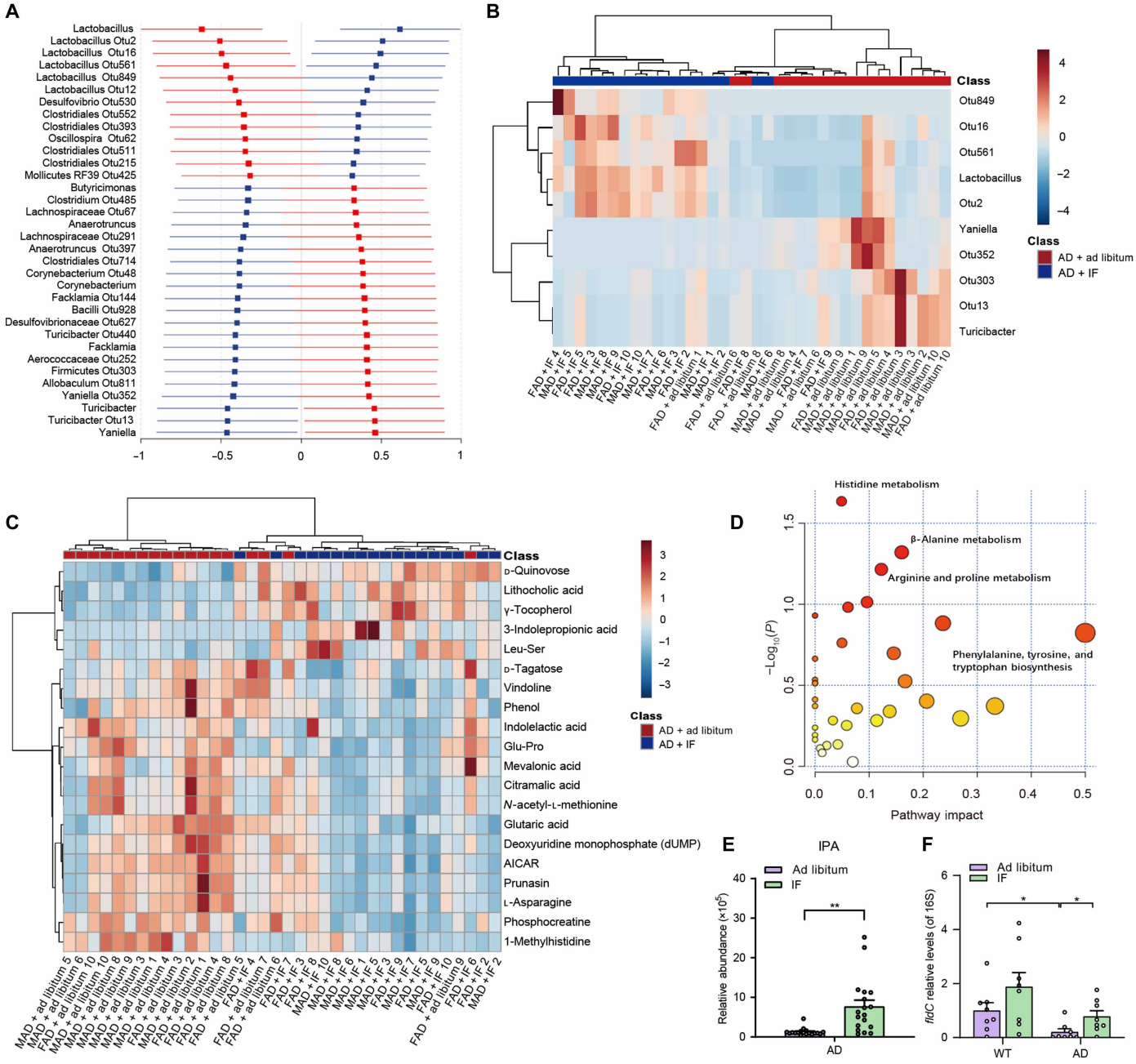

Fig. 2. IF restructured the gut microbiome and metabolome of AD mice. (**A**) Differences in a selection of six genera and 28 OTUs differed between AD + ad libitum and AD + IF groups. The least-square means ±95% confidence intervals obtained from ANOVA ($P < 0.05$) are presented. (**B**) A *z*-score scaled heatmap of top 10 bacteria that differed between AD + ad libitum and AD + IF with $P < 0.05$. (**C**) A *z*-score scaled heatmap of differential metabolites between AD + ad libitum and AD + IF with $P < 0.05$. The top 20 differential metabolites are presented. (**D**) Metabolic pathways influenced by IF treatment in AD mice (AICAR, 5-Aminoimidazole-4-carboxamide1-β-D-ribofuranoside). (**E**) Plasma levels of IPA ($n = 18$). (**F**) DNA level of *fldC* in colon content ($n = 8$). Data are mean ± SEM. *$P < 0.05$ and **$P < 0.01$. Statistical significance for (E) and (F) was determined by two-way ANOVA followed by Tukey's multiple comparisons test.

respectively, with 77 metabolites in common (fig. S3A). Univariate statistics revealed 87 differential AD + ad libitum versus AD + IF metabolites (Fig. 2C and fig. S3C) showing varying degrees of correlations with each other (fig. S3B). These metabolites were enriched in the metabolism of histidine, β-alanine, arginine, and proline (Fig. 2D). Of note, 10 metabolites have been associated with AD development and/or cognitive impairment (Fig. 2E and fig. S3D). Metabolites involved in the tryptophan metabolic pathway have been considered gut microbiota–related metabolites, including IPA and indolelactic acid (Fig. 2E and fig. S3D). The *fldC* gene, encoded by gut microbiota and responsible for phenylactyl-CoA dehydratase—an enzyme essential for IPA biosynthesis—was significantly up-regulated in the gut of AD mice following IF intervention. (Fig. 2F). Thus, IF restructured the gut microbiome, modified

metabolic pathways—particularly tryptophan metabolism—and increased the levels of IPA in AD mice.

Multiomics integration for IF on AD mice

We identified 175 hippocampal genes, 34 gut bacterial species, and 87 plasma metabolites as key signatures associated with IF treatment in AD mice. To explore their potential mechanistic connections, we analyzed the interplay among these features (Fig. 2). Genes, gut bacteria, and metabolites distinguished AD + IF from AD + ad libitum with accuracies of 92, 100, and 92%, respectively (Fig. 3A). Predictions were made using partial least squares discriminant analysis with a repeated double cross-validation framework to minimize overfitting. The models' predictive ability surpassed 1000 permuted models, demonstrating their robustness and generalizability (Student's *t* test, $P < 0.05$). We used DIABLO (Data Integration Analysis for Biomarker discovery using a Latent component method for Omics) integration analysis with a weighted design (fig. S4A) to identify biologically relevant and highly correlated omic signatures (fig. S4B). Figure 3 summarizes the integrative analysis of IF-modulated gut microbes, metabolites, and hippocampal genes. A total of 28 genes, 32 bacteria, and 40 metabolites were identified as key omic signatures differentiating AD + ad libitum from AD + IF groups (Fig. 3B). Fig. 3 (C to E) illustrates the loading scores of predictors from gut microbes, plasma metabolites, and hippocampal genes, highlighting their contributions to differentiating AD + ad libitum and AD + IF groups. Notably, following IF intervention, the gut microbes *Ruminococcus* and *Lactobacillus*, the serum metabolite IPA, and the expression of hippocampal gene *Zfyve1* were not only significantly up-regulated but also exhibited the greatest differences between treatment groups. These features emerged as the top-ranking contributors to the observed

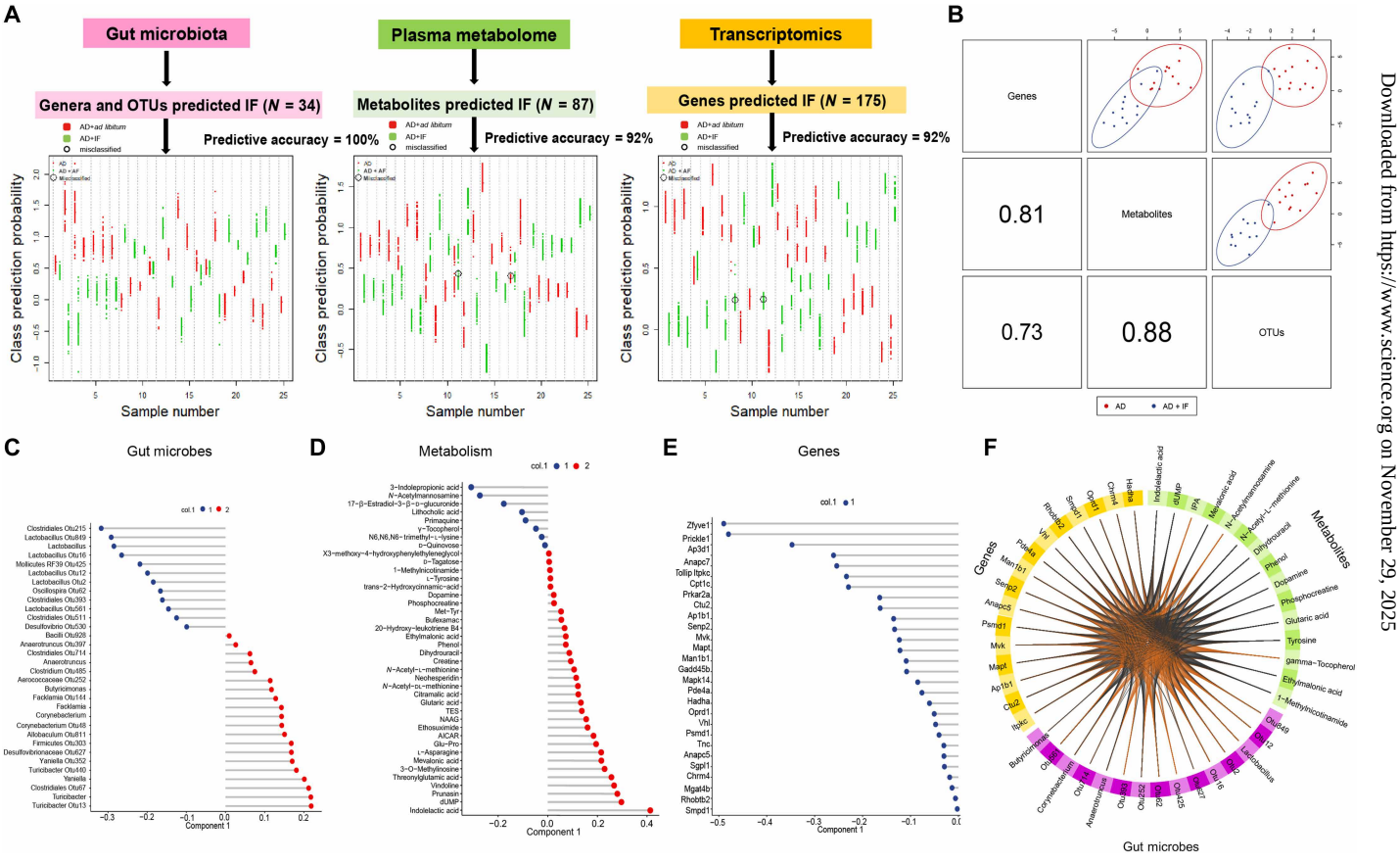

Fig. 3. Multiomics integration for IF treatment. (**A**) The performance of predictive models for signatures of IF status. Omic signatures included 175 differential AD + ad libitum versus AD + IF genes expressed in the hippocampus, 34 gut bacteria, and 87 plasma metabolites. For each dataset, multivariate predictive modeling was conducted using partial least squares discriminant analysis incorporated into a repeated double cross-validation framework. Prediction performance is shown in downstream figures: Each swim lane represents one mouse. For each sample, class probabilities were computed from 200 double cross-validations. Class probabilities are color-coded by class, presented per repetition (smaller dots), and averaged over all repetitions (larger dots). Misclassified samples are circled. Predictive accuracy was calculated as the number of correctly predicted samples/total number of measured samples. (**B**) Model performance of DIABLO integrative analysis of omic signatures concerning IF. The use of DIABLO maximized the correlated information between genes, bacteria, and metabolites. Scatterplots depicting the clustering of groups, i.e., AD + ad libitum and AD + IF, based on the first component of each dataset from the model, showed significant separation between groups. A scatterplot displays the first component in each dataset (top diagonal plot) and Pearson correlation between components (bottom diagonal plot). (**C** to **E**) Lollipop plot of contributions of key omic signatures identified by DIABLO integrative modeling for discriminating AD + IF from AD + ad libitum. Loading of DIABLO integrative modeling for each predictor is presented. Blue bars indicate IF-induced improvements in predictors. Predictors that were lower in AD + IF compared with AD + ad libitum are in red. TES, N-Tris(hydroxymethyl)methyl-2-aminoethanesulfonic acid sodium salt hydrate; NAAG, N-acetylaspartylglutamate. (**F**) The Circos plot shows the positive (negative) correlation, denoted as brown (gray) lines, between selected multiomics features.

multiomics associations across the microbiome, metabolome, and transcriptome. In addition, the selected omic signatures displayed strong interrelationships, as shown in Fig. 3F. In addition to strong interrelationships among genes, bacteria, and plasma metabolites, we observed significant correlations between key predictors and IF-induced improvements in escape latency during navigation tests ($r = 0.51$, 0.50, and 0.45 for genes, gut bacteria, and plasma metabolites, respectively).

The neuroprotective effects of IF are mediated by gut microbiota

To determine whether gut microbiota contribute to the cognitive improvements observed in AD mice with IF, we conducted further analyses. Ten-month-old AAPswe/PS1dE9 male mice and WT littermates received an antibiotic mixture [ABx; penicillin G sodium (1 g/liter), metronidazole (1 g/liter), neomycin sulfate (1 g/liter), streptomycin sulfate (1 g/liter), and vancomycin hydrochloride (0.5 g/liter)] for 2 weeks, followed by IF treatment for 6 weeks (Fig. 4A). ABx treatment significantly reduced the 16*S* rRNA gene copy numbers in feces (fig. S5A). IF decreased body weight and food intake in AD mice but had no effect on water intake (Fig. 4B and fig. S5, B to D). Compared with the AD + IF group, the AD + IF + ABx group showed no significant changes in body weight, food intake, or weekly water intake (Fig. 4B and fig. S5, C and D). To evaluate the cognitive function of ABx- and/or IF-treated AD mice while avoiding microbial contamination from swimming water, we used the Barnes maze test instead of the water maze test. During acquisition and probe trials, the primary latency of AD mice increased with training days compared to WT mice (Fig. 4C and fig. S5E). IF significantly enhanced cognitive performance in AD mice. In contrast, the AD + IF + ABx group exhibited a significantly longer primary latency compared to the AD + IF group, suggesting that the cognitive benefits of IF were partially mitigated by gut microbiota removal (Fig. 4C and fig. S5, E and F).

The influence of ABx on the beneficial effects of IF was investigated by comparing the AD + IF + ABx group and the AD + IF group. As shown in Fig. 4 (E to G), the beneficial effects of IF on Aβ deposition were eliminated by ABx treatment. Similarly, ABx treatment abolished the IF-induced down-regulation of *TNF*α, *APP*, and *Bace-1* mRNA expression, as well as the up-regulation of *PSD-95* and *IL-10* mRNA expression (Fig. 4D and fig. S5, G to J).

The omic study revealed that the microbial metabolite IPA was up-regulated following IF treatment in AD mice, suggesting that IPA plays a key role in mediating IF's neuroprotective effects. To block the beneficial effects of IPA, 10-month-old male APP/PS1 mice were intraperitoneally administered ketoconazole (KCZ; 0.05 mg/kg per day), an inhibitor of the IPA receptor, pregnane X receptor (PXR) (Fig. 4H). The results indicated that KCZ did not influence the body weight, food intake, or water intake of IF-treated AD mice (fig. S5, K to M). However, KCZ injection partially abolished the protective effects of IF on cognitive function in AD mice, as assessed by the Barnes maze test (Fig. 4, I and J). Similarly, KCZ injection increased Aβ accumulation in the piriform cortex and hippocampus of IF-treated AD mice (Fig. 4, K to M). KCZ injection did not alter the IPA levels in the feces or serum of IF-treated mice (fig. S5, N and O). KCZ injection inhibited the mRNA expression of *Cyp3a11*, a downstream gene of PXR (fig. S5P). Consistent with the behavioral and Aβ results, KCZ increased mRNA expression of *APP* and tumor necrosis factor–α (*TNF*α) while decreasing the expression of *PSD-95* and *IL-10* (Fig. 4N and fig. S5, Q to S).

These findings suggest that gut microbiota, particularly the microbial metabolite IPA, play a vital role in the neuroprotective effects of IF on AD mice.

IPA mimics the neuroprotective effects of IF

To further investigate the potential benefits of IPA in AD, we measured serum IPA levels in human volunteers, including patients with AD, patients with mild cognitive impairment (MCI), and healthy individuals (Fig. 5A). Serum IPA levels were significantly lower in the MCI and AD groups compared to healthy controls, consistent with fecal IPA levels (Fig. 5, B and C). Serum IPA levels were significantly correlated with cognitive scores, including the Montreal Cognitive Assessment (MoCA; $r = 0.71$, $P < 0.0001$) and the Mini-Mental State Examination (MMSE; $r = 0.59$, $P < 0.0001$) (Fig. 5, D and E). Moreover, the relative abundance of the *fldC* gene in the gut microbiota of individuals with AD was significantly lower than that observed in healthy controls and individuals with MCI (fig. S6C). Correlation analysis revealed a strong positive association between the relative abundance of *fldC* and serum levels of IPA ($r = 0.80$, $P < 0.0001$) (fig. S6D).

To validate the neuroprotective effects of IPA, 5-month-old male APP/PS1 mice were treated with IPA (20 mg/kg per day, gavage) for 6 weeks (Fig. 5F). The Barnes maze test demonstrated that IPA significantly improved cognitive function in AD mice (Fig. 5G). The novel object recognition (NOR) test showed that IPA enhanced recognition memory in AD mice (Fig. 5H). IPA treatment appeared to eliminate Aβ accumulation in the piriform cortex and hippocampus of AD mice (Fig. 5, J to L). IPA supplementation markedly increased serum IPA levels but had no effect on fecal IPA levels in AD mice (fig. S6, E and F). IPA down-regulated the mRNA expression of *APP* and *TNF*α while up-regulating *Cyp3a11*, *PSD-95*, and *IL-10* (Fig. 5I and fig. S6, G to J).

Clostridium sporogenes, a well-known gut bacterium, is capable of generating IPA in the host (*29*). We treated 7-month-old male 5×FAD mice with *C. sporogenes* or a mutant strain to confirm the role of gut-derived IPA in cognitive regulation (Fig. 5M). The *C. sporogenes* △*fldC* mutant strain lacked the *fldC* gene. In vitro experiments confirmed that the mutant *fldC* strain was incapable of generating IPA in the culture medium (Fig. 5N). The 5×FAD transgenic AD mice were treated with WT or mutant *C. sporogenes* for 28 days after a 3-day vancomycin regimen to eliminate other gut bacteria–producing tryptophan metabolites (*22*). At the conclusion of the experiments, IPA was undetectable in the feces of mice colonized with the *C. sporogenes* △*fldC* mutant strain (Fig. 5O). The mRNA expression levels of *Mdr1a* and *Cyp3a11* were reduced in the brains of AD mice treated with the mutant strain (fig. S6, K and L). Behavioral tests, including the NOR and Y-maze tests, revealed that mice colonized with *C. sporogenes* △*fldC* exhibited significantly lower discrimination indices and spontaneous alternation rates in the Y-maze compared to those colonized with the WT strain (Fig. 5, P and R). Consistently, treatment with *C. sporogenes* △*fldC* resulted in greater Aβ accumulation in the piriform cortex and hippocampus of AD mice and elevated *Bace-1* mRNA expression in the hippocampus compared to mice recolonized with the WT strain (Fig. 5, Q, S, and T, and fig. S6P). Similarly, treatment with the mutant bacteria led to higher levels of microglial activation (fig. S6, M to O). These findings suggest that IPA exerts preventive effects on Aβ accumulation, neuroinflammation, and cognitive dysfunction in AD mice.

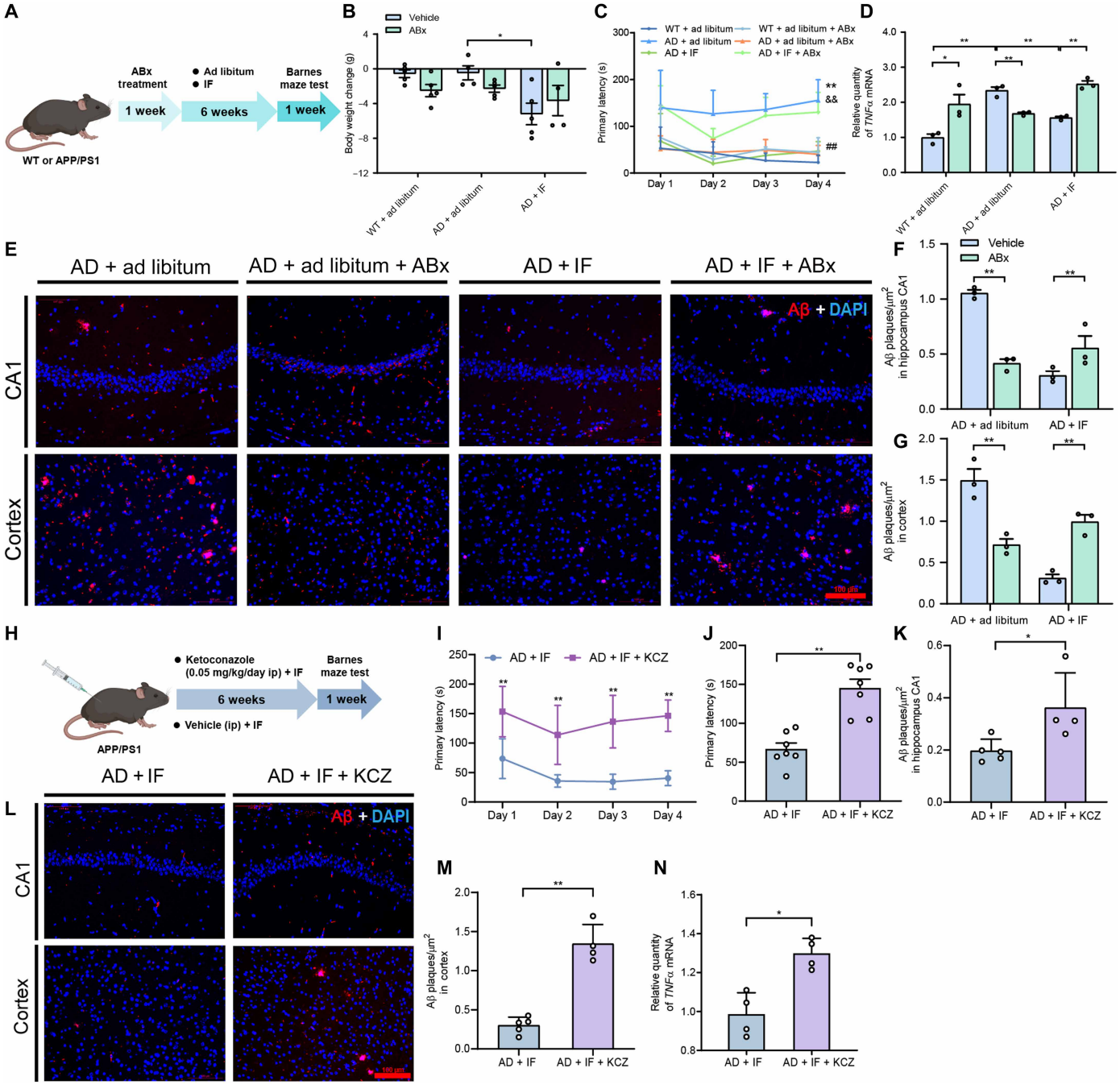

Fig. 4. The neuroprotective effects of IF are mediated by gut microbiota. For antibiotic administration experiment: (**A**) Schematic of the treatment with ABx and IF in each group ($n = 4$ to 5). (**B**) Body weight change (WT + ad libitum, WT + ad libitum + ABx, AD + ad libitum + ABx, and AD + IF: $n = 5$; AD + ad libitum and AD + IF + ABx: $n = 4$). (**C**) Primary latency in acquisition trials of Barnes maze [same group sizes as in (B)]. (**D**) Hippocampal *TNFα* mRNA levels ($n = 3$). (**E**) Representative immunofluorescence of Aβ plaques in the hippocampal CA1 region and piriform cortex ($n = 3$ slices per group). Scale bar, 100 μm. (**F** and **G**) Aβ plaque density (number of plaques per square micrometer) in the hippocampal CA1 region and piriform cortex ($n = 3$ mice per group). For ketoconazole (intraperitoneal) injection experiment: (**H**) Schematic of the treatment with KCZ (intraperitoneal) and IF in each group ($n = 7$). (**I**) Primary latency in Barnes maze acquisition trials ($n = 7$). (**J**) Primary latency in probe trial of Barnes maze ($n = 6$). (**K**) Aβ plaque density (number of plaques per square micrometer) in the CA1 region of the hippocampus (AD + IF: $n = 5$, AD + IF + KCZ: $n = 4$). (**L**) Representative immunofluorescence images of Aβ plaques in the piriform cortex and CA1 region of the hippocampus [same group sizes as in (K)]. Scale bar, 100 μm. (**M**) Aβ plaque density (number of plaques per square micrometer) in the piriform cortex [same group sizes as in (K)]. (**N**) Hippocampal *TNFα* mRNA levels ($n = 4$). In (C), * indicates a significant difference between WT + ad libitum and AD + ad libitum, # indicates a significant difference between AD + ad libitum and AD + IF, and & indicates a significant difference between AD + IF + ABx and AD + IF. Data are mean ± SEM. $^{*}P < 0.05$, $^{**}P < 0.01$, $^{\#\#}P < 0.01$, and $^{\&\&}P < 0.01$. For the antibiotic experiment [(B) to (G)], statistical significance was determined by one-way ANOVA followed by Tukey's multiple comparisons test. For the KCZ experiment [(I) to (N)], comparisons between the two groups were performed using a Student's *t* test.

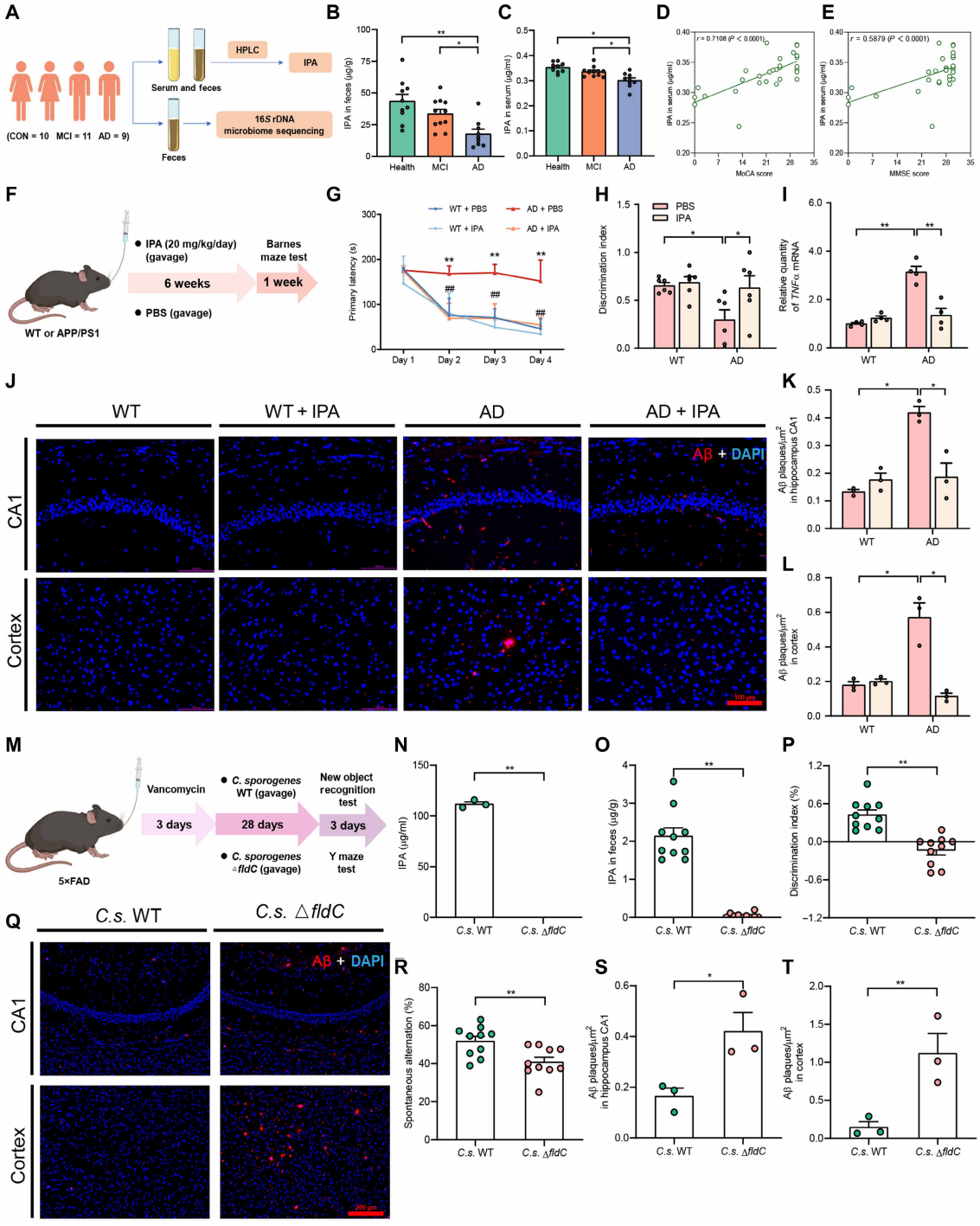

Fig. 5. IPA mimics the neuroprotective effects of IF. Human data: (**A**) Workflow for collection and processing of samples. (**B**) Fecal IPA concentrations ($n = 9$ to 11). (**C**) Serum IPA concentrations ($n = 9$ to 11). Correlation between serum IPA and (**D**) MoCA or (**E**) MMSE scores. For IPA (gavage) experiment: (**F**) Schematic of the IPA treatment ($n = 6$). (**G**) Primary latency in Barnes maze acquisition trials ($n = 6$). (**H**) Discrimination index in the novel object recognition (NOR) test ($n = 6$). (**I**) Hippocampal TNFα mRNA expression ($n = 4$). (**J**) Representative immunofluorescence of Aβ plaques in the piriform cortex and CA1 region of the hippocampus ($n = 3$ slices per group). Scale bar, 100 μm. (**K** and **L**) Aβ plaque density (number of plaques per square micrometer) in the CA1 region of the hippocampus and piriform cortex. For the *C.S.* WT or *C.S.* △*fldC* recolonization experiment: (**M**) Schematic of the treatment with vancomycin and *C.S.* WT or *C.S.* △*fldC* ($n = 10$). The content of IPA in the (**N**) culture medium ($n = 3$) and (**O**) mouse serum ($n = 9$ to 10). (**P**) Discrimination index in the NOR test ($n = 9$ to 10). (**Q**) Representative immunofluorescence images of Aβ plaques in the piriform cortex and CA1 region of the hippocampus ($n = 3$ slices per group). Scale bar, 200 μm. (**R**) The spontaneous alternation of the Y-maze test ($n = 9$ to 10). (**S** and **T**) Aβ plaque density (number of plaques per square micrometer) in the CA1 region of the hippocampus and piriform cortex. Data are mean ± SEM. $^*P < 0.05$ and $^{**}P < 0.01$. For human data [(B) and (C)], significance was determined by one-way ANOVA with Tukey's test. For the IPA gavage experiment [(G) to (L)], a two-way ANOVA with Tukey's test was used. For the *C. sporogenes* colonization experiment [(N) to (T)], a Student's *t* test was used for comparisons between the two groups.

IPA attenuates neuroinflammation by activating PXR

To confirm that IPA can penetrate the BBB (*30*), we conducted dynamic experiments and observed detectable IPA levels in the brain within 1 hour postinjection, peaking at the same time (fig. S7, A and B). Similarly, serum IPA levels also peaked 1 hour postinjection (fig. S7C).

We performed intracerebroventricular (i.c.v.) injections of KCZ to block the IPA's receptor, PXR, in the hippocampus. Nine-month-old male 5×FAD mice were then treated with IPA (20 mg/kg per day, intraperitoneally) for 14 days, following a 3-day vancomycin regimen to deplete gut bacteria primarily responsible for IPA production (fig. S7D). The NOR and Y-maze tests demonstrated that IPA treatment significantly alleviated cognitive dysfunction in AD mice (fig. S7, E and F). However, KCZ (i.c.v.) injections nullified the cognitive benefits of IPA treatment. In addition, KCZ abolished IPA's protective effects against Aβ accumulation in the hippocampus and piriform cortex (fig. S7, H to J) and reversed IPA-mediated down-regulation of *TNF*α, *COX2*, and *Bace-1* mRNA expression in the brain (fig. S7, G, K, and L). KCZ injection did not affect serum IPA levels (fig. S7M) but suppressed the mRNA expression of *Mdr1a/b* and *Cyp3a11*, thereby inhibiting PXR activation (fig. S7, N to P). Thus, these results further confirmed that IPA could penetrate the BBB and suppress neuroinflammation by activating PXR in neurons.

IPA suppresses NFκB/Bace-1 activation by activating PXR in neurons

To determine the cell type–specific localization of PXR in the brain, we performed double immunofluorescent staining of PXR and neuronal cell markers, including neuron-specific nuclear protein (NeuN; an neuron-specific marker), glial fibrillary acidic protein (GFAP; an astrocyte-specific marker), or IBA-1 (a microglia-specific marker) in the mouse brain. The staining results indicated that PXR was only highly expressed in $NeuN^+$ neurons, but not in $GFAP^+$ astrocytes and $IBA\text{-}1^+$ microglia (fig. S8A). On the basis of the above findings and to further delineate the cell type specificity of IPA's function, we constructed an adeno-associated virus (AAV) in which an PXR-targeting short hairpin RNA (shRNA) was expressed under the control of the hSyn promoter (PXR-shRNA) and used it to specifically knock down PXR expression in neurons of 9-month-old male 5×FAD mice (Fig. 6A). As shown in fig. S8 (B and C), the AAV successfully infected the neurons in the hippocampus and decreased the effective expression of PXR in neurons. Consistent with the results of KCZ i.c.v. injection, hippocampal delivery of PXR-shRNA abolished the protective effects of IPA on cognitive impairment (Fig. 6, B and C) and Aβ accumulation in AD mice (Fig. 6, D to F). Moreover, IPA markedly reduced both mRNA and protein levels of *Bace-1* in the hippocampus of AD mice, which was effectively reversed by PXR-shRNA intervention (Fig. 6, G and I). IPA also up-regulated the expression of Cyp3a11 and Mdr1, downstream of PXR (Fig. 6, L to M, and fig. S8D). However, these effects were similarly abrogated following PXR deficiency in neurons. As shown in Fig. 6N, IPA significantly lowered the phosphorylated nuclear factor κB (p-NFκB)/NFκB ratio and reduced the mRNA expression of *TNF*α and *COX2* in the hippocampus of AD mice (Fig. 6O and fig. S8E). However, the anti-inflammatory effects of IPA were attenuated in PXR-deficient mice. Inhibition of NFκB phosphorylation has been reported to reduce Bace-1 activity and subsequently decrease Aβ deposition in the brains of AD mice (*31*, *32*). These findings suggest that IPA may attenuate Aβ production by suppressing NFκB activation and Bace-1 expression, predominantly within neurons.

We found that serum TNFα levels were significantly elevated in individuals with AD, consistent with an enhanced neuroinflammatory state (fig. S9A). On the basis of the above findings, to further confirm the concurrent inhibitory effects of IPA on NFκB phosphorylation and Bace-1 expression, we used a TNFα (20 ng/ml)–induced neuroinflammation model in SH-SY5Y human neuroblastoma cells to examine whether IPA could inhibit Bace-1 expression. We found that IPA attenuated TNFα (20 ng/ml)–induced down-regulation of Mdr1, the increased p-NFκB/NFκB ratio, and up-regulation of Bace-1 expression in SH-SY5Y human neuroblastoma cells (fig. S9, D to G). Furthermore, we performed a model by (i.c.v.) injection of TNFα into the hippocampus of C57BL/6J mice, after intraperitoneal administration of IPA (Fig. 6P). Y-maze test results showed that IPA injection before surgery significantly increased the spontaneous exploration rate in TNFα-treated mice (Fig. 6Q). IPA also up-regulated the mRNA expression of *Mdr1b* (Fig. 6R) and down-regulated the content of TNFα and the expression of Bace-1 in the hippocampus (Fig. 6S and fig. S9H). Thus, these results further confirmed that IPA suppresses NFκB activation and inhibits Bace-1 expression through neuronal PXR activation, thereby reducing Aβ accumulation and improving cognitive impairment in mice. This mechanism may provide insight into how IPA down-regulates Aβ accumulation and reverses cognitive dysfunction.

DISCUSSION

Here, we observed that IF enhanced cognitive function and spatial memory, concurrently attenuating Aβ accumulation in the piriform cortex and hippocampus of APP/PS1 mice. IF notably modified gene expression related to autophagy, synaptic plasticity, and cognitive function in the hippocampus of AD mice. In addition, IF enhanced gut barrier integrity, altered the gut microbiome, and subsequently augmented the production of neuroprotective microbial metabolites. Our integrated analysis of gene expression, gut microbiome, and metabolites suggests that 16 weeks of IF ameliorated cognitive deficits in AD mice, primarily through the gut-brain axis, with IPA potentially being a crucial microbial metabolite. Pseudo germ-free mice were used to further demonstrate a pivotal function of gut microbiota in regulating the neuroprotective effects of IF in AD mice. Blocking the IPA receptor PXR also nullified the neuroprotective effects of IF. Human data revealed reduced IPA levels in patients with MCI and AD relative to healthy individuals. Supplementation of IPA and IPA-producing bacteria *C. sporogenes* could mimic IF's effects, but blocking the PXR in the brain or knocking of the IPA-producing gene *fldC* in the *C. sporogenes* also eliminated these effects. IPA could penetrate the BBB, and IPA may have neuroprotective effects due to its anti-inflammatory properties, according to TNFα (i.c.v.) injection experiment. Therefore, these results suggest that IF protects against cognitive dysfunction in AD by altering the composition of the gut microbiota, in which IPA is a pivotal metabolite.

In addition to the above findings, aside from genetic factors, environmental factors, such as diet, can also influence AD development (*4*). Prior research has demonstrated that IF enhances spatial learning and memory across different transgenic AD mouse models, including APP mutant, 3xTgAD, and APP/PS1 mice (*10*, *13*, *16*, *33*). We observed a significant improvement in the cognitive function of APP/PS1 mice following IF treatment, as measured by behavioral tests (Fig. 1). Despite some resistance and controversy surrounding the "amyloid cascade hypothesis," Aβ's involvement in the onset and

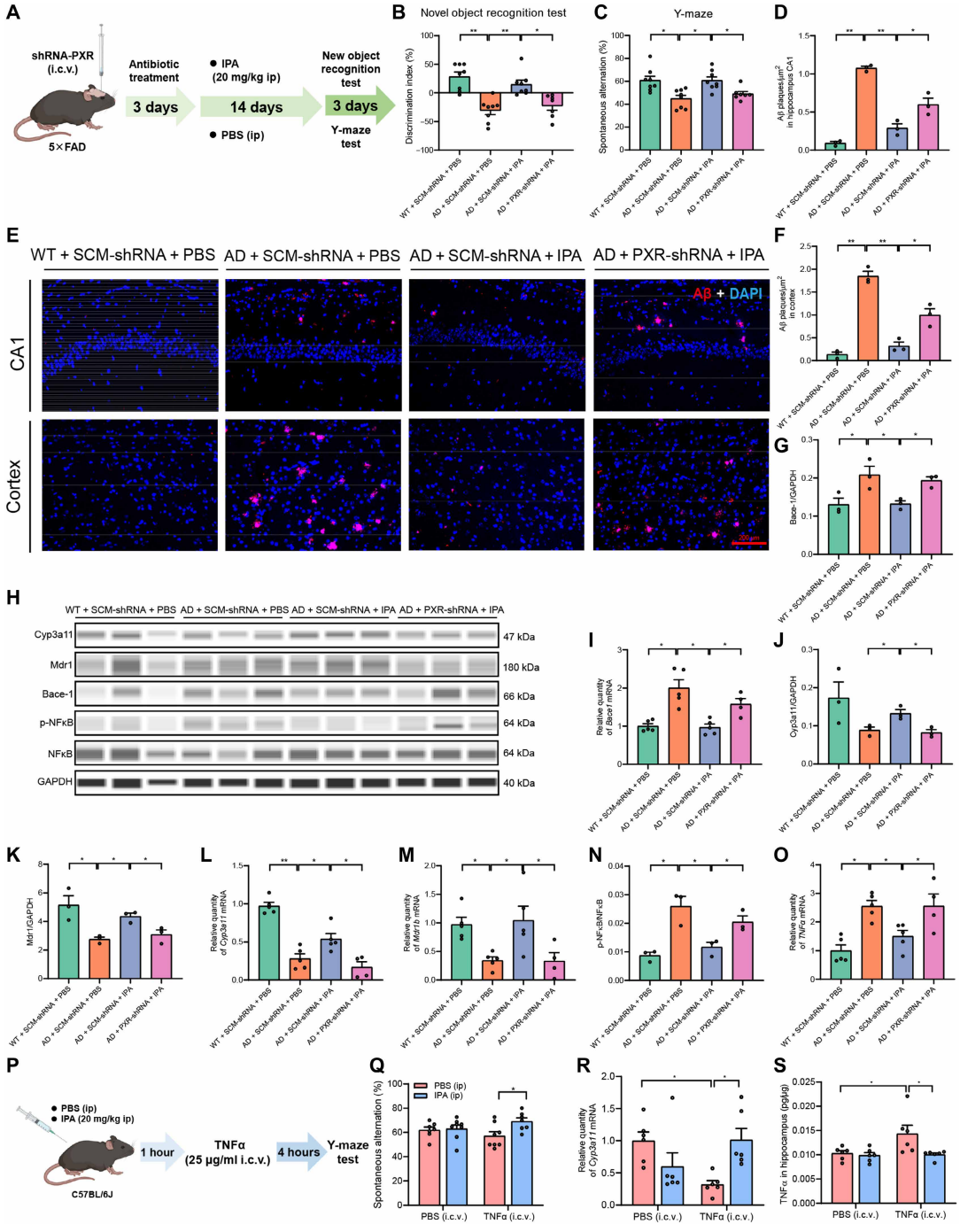

Fig. 6. IPA attenuates neuroinflammation via activating PXR. For PXR-shRNA (i.c.v.) experiment: (**A**) Schematic of the treatment with PXR-shRNA (i.c.v.) and IPA in each group ($n = 8$). (**B**) Discrimination index in the NOR test and (**C**) spontaneous alternation in the Y-maze test ($n = 7$ to 8), SCM-shRNA, mice were treated with AAV-scrambled shRNA (negative control). (**D** and **F**) Quantification of Aβ plaque density in the CA1 region and piriform cortex (plaques per square micrometer). (**E**) Representative immunofluorescence images of Aβ plaques in CA1 ($n = 3$ slices per group). Scale bars, 200 μm. (**G**) Quantification of the Western blot of Bace-1 protein levels relative to glyceraldehyde phosphate dehydrogenase (GAPDH) in the hippocampus ($n = 3$). (**H**) Representative Western blot of Bace-1, Cyp3a11, Mdr1, p-NFκB, NFκB, and GAPDH protein levels in the hippocampus ($n = 3$). (**I**) The mRNA levels of *Bace-1* in the hippocampus ($n = 4$ to 5). (**J** and **K**) Quantification of the Western blot of Cyp3a11 and Mdr1 protein levels relative to GAPDH in the hippocampus ($n = 3$). (**L** and **M**) The mRNA levels of *Cyp3a11* and *Mdr1b* in the hippocampus ($n = 4$ to 5). (**N**) Quantification of the Western blot of p-NFκB protein levels relative to NFκB in the hippocampus ($n = 3$). (**O**) The mRNA levels of *TNFα* in the hippocampus ($n = 4$ to 5). For TNFα (i.c.v.) experiment: (**P**) Schematic of the treatment with *TNFα* (i.c.v.) and IPA in each group ($n = 7$ to 8). (**Q**) The spontaneous alternation of the Y-maze test ($n = 7$ to 8). (**R**) The mRNA levels of *Cyp3a11* in the hippocampus ($n = 6$). (**S**) *TNFα* content in the hippocampus ($n = 6$). Data are mean ± SEM. $^*P < 0.05$ and $^{**}P < 0.01$. For the PXR-shRNA and TNFα injection experiments, which involved comparisons across four groups [(B) to (D), (G), (I) to (O), and (Q) to (S)], statistical significance was determined by one-way ANOVA followed by Tukey's multiple comparisons test.

progression of AD is well documented (*34*). Furthermore, increased levels of Aβ and highly phosphorylated tau proteins are recognized as significant biomarkers and predictors of early-stage dementia (*35*). Our findings indicated that IF might attenuate excessive Aβ accumulation in the piriform cortex and hippocampal CA1 regions of AD mice while significantly decreasing APP expression in the hippocampus (Fig. 1). IF's reduction of Aβ deposition in AD mouse brains suggests its potential benefits in AD prevention. Accumulation of Aβ in the brain is caused by an imbalance in the production and clearance of Aβ, and autophagy is an important mechanism of Aβ clearing (*36*). We observed an increase in autophagy-related gene expression, such as *ZFYVE1*, *Lamp2*, and *Foxo6*, in the hippocampus of AD mice following IF (Fig. 2). This finding may partly explain the beneficial effects of IF on Aβ deposition. Moreover, IF up-regulated the expression of *Gadd45b*, a regulator of neurogenesis, as well as *Ap3d1* and *Cpt1c* (Fig. 2) (*37*). Our study revealed that IF significantly preserved the ultrastructure of synapses in hippocampal neurons and increased the expression of genes related to synaptic plasticity, such as *PSD-95* and *Ap3d1* (*38*).

Gut dysbiosis and increased intestinal permeability are implicated in neuroinflammatory responses within the central nervous system (CNS) and an increased risk of AD (*39*, *40*). Studies suggest that gut dysbiosis exacerbates neuroinflammation in neuronal C/EBPβ transgenic mouse models (*41*). Dietary interventions, such as caloric restriction (CR) and IF, have been shown to mitigate Aβ accumulation in AD mice, an effect partly attributable to alterations in gut microbiota composition (*16*, *42*). Our prior studies indicated that IF may prevent diabetes-associated cognitive decline by modulating gut microbiome composition and metabolic functions (*9*). Consistently, our findings reveal that IF significantly alters the relative abundance of cognitively associated bacteria, including *Lactobacillus*, *Corynebacterium*, and *Allobaculum* (Fig. 3 and fig. S2). *Lactobacillus* has been demonstrated to mediate the anti-inflammatory and metabolic benefits of both long-term and short-term CR (*43*, *44*). Lactobacillus supplementation mitigated cognitive dysfunction and corrected abnormal fear memory in an animal model of autism (*45*) and enhanced spatial memory and learning in postoperative neurocognitive disorders (*46*). In addition, oral probiotics containing *Lactobacillus reuteri* enhanced spatial memory, diminished Aβ plaque burden, and lowered inflammatory markers *IL-1*β and *TNF*α in AD rats subjected to intrahippocampal $A\beta_{1-40}$ injections (*47*). Conversely, IF was associated with a down-regulation of *Butyricimonas* and *Allobaculum* levels (Fig. 3). Recent studies have indicated a negative correlation between the relative abundance of *Butyricimonas* and human cognitive ability (*48*). However, in our previous research, *Allobaculum* was reduced in IF-treated diabetic mice (*9*). Removal of gut microbiota with ABx treatment (Fig. 4) significantly abolished the beneficial effects of IF on AD. Of note, a reduction in cerebral Aβ accumulation was observed in ad libitum–fed AD mice that received ABx treatment, which may be associated with decreased hippocampal *TNF*α expression (Fig. 4). Similarly, previous work has shown that long-term administration of broad-spectrum combinatorial or single antibiotics lessens Aβ plaque deposition, likely through diminishing harmful bacteria and neuroinflammation in AD mice (*49*, *50*). Thus, these results suggest that IF prevents cognitive dysfunction in AD by modulating the gut microbiota composition. Future research should explore potential probiotics derived from healthy individuals or engineered to simulate the effects of dietary restrictions and use optimized fecal microbiota transplantation methods to investigate the potential role of microbial interventions in improving AD.

Integrated multiomics analysis reveals that IPA is the key metabolite affected by IF treatment. IPA, a tryptophan-derived microbial metabolite previously mentioned, is widely reported to have neuroprotective effects. The production of IPA is associated with the presence of specific gut microbiota, particularly *C. sporogenes* (*29*, *51*). *Lactobacillus* species, including *L. reuteri* and *Lactobacillus johnsonii*, can also metabolize intestinal tryptophan into indole-3-lactic acid (ILA), which serves as a key precursor for IPA synthesis by *C. sporogenes* (*51*). Therefore, the IF-induced increase in *Lactobacillus* may promote IPA production by supplying more ILA substrate to *C. sporogenes*. Whether *Corynebacterium*, *Allobaculum*, or *Butyricimonas* influence *C. sporogenes* or other IPA-producing bacteria through cross-feeding interactions within the gut microbiota remains unclear and warrants further investigation to clarify these complex relationships. Recent studies suggest that IPA alleviates Aβ fibril formation and propose it as a candidate for treating metabolic disorders by lowering fasting blood glucose and reducing insulin resistance (*23*, *52*). IPA has been found to reduce proinflammatory cytokine levels in lipopolysaccharide-activated astrocytes (*53*). Our earlier study demonstrated that IPA supplementation could replicate IF's beneficial effects in an animal model of diabetes-associated cognitive dysfunction. A recent human study revealed that probiotic treatment can enhance IPA production, elevate brain-derived neurotrophic factor expression, and reduce neuroinflammation (*25*). Several in vivo and in vitro studies have also shown that IPA can down-regulate the NFκB pathway, subsequently suppressing inflammatory cytokines such as TNFα (*24*, *29*, *46*, *54*). Bace-1 cleavesAPP to generate Aβ, a key component of neuritic plaques in AD brains (*55*). Inhibition of NFκB phosphorylation has been reported to reduce Bace-1 activity and decrease Aβ accumulation in the brains of AD mice (*30*, *31*). Notably, in a 5×FAD transgenic mouse model, alternate-day fasting worsened neuroinflammation and increased TNFα protein levels (*33*). Consistently, we found that either IPA alone or *C. sporogenes*, an IPA-producing bacterium, could replicate IF's beneficial effects in AD mice. These effects were nullified by PXR inhibitors and neuron-specific knockout of PXR, the receptor for IPA. The knockout also down-regulated the NFκB pathway and Bace-1 expression in AD mice. These data suggest that IPA is the critical metabolite mediating IF's beneficial effects on AD. In addition, we performed a dose-response study of IPA in a TNFα-induced acute neuroinflammation model, revealing that IPA's ameliorative effects on cognitive impairment and neuroinflammation are dose dependent. Notably, the dose of 20 mg/kg effectively activated PXR downstream targets and reduced the expression of inflammatory markers and Bace-1 [see fig. S10 (A to J)]. At the same time, KCZ can inhibit other enzymes, such as cyclosporine oxidase; therefore, it remains unclear whether IPA can bind to other receptors and exert its beneficial effects on AD. Our recent work also established that, compared to time-restricted feeding and intermittent energy restriction, alternate-day fasting aggravated dextran sulfate sodium–induced colitis and inflammation in a chronic colitis mouse model (*56*). The disparity in findings underscores the need for further research to elucidate IF regimen effects across various animal models and human trials. Supplementation with probiotics or key metabolites could potentially emulate the benefits of dietary restriction more effectively than IF alone. Notably, participants in alternate-day fasting studies reported irritability on fasting days (*57*), potentially limiting its clinical use. It may be preferable to adopt more moderate and sustainable time-restricted fasting in the future.

In summary, this study reveals that IF significantly enhances cognitive function in AD mice, concomitant with reduced Aβ accumulation and neuroinflammation in the CNS. The cognitive benefits of IF in AD may stem from the gut-brain axis, whereby IF modifies the gut microbiome and boosts metabolite production, like IPA, preventing neuroinflammation and Aβ buildup in the CNS. These findings strongly support the potential for therapeutic and nonpharmacological nutritional interventions in AD and other neurodegenerative disorders.

MATERIALS AND METHODS

Human study

In collaboration with Peking University Shenzhen School of Medicine's Neurology Department, participants, upon admission, undergo the following assessments: (i) MMSE and MoCA to evaluate comprehensive cognitive function; (ii) a medical interview to confirm medical history and current medication use; (iii) the analysis of the four cerebrospinal fluid components (including Aβ1-40, Aβ1-42, t-Tau, and p-Tau, voluntary participation), which serve as the diagnostic basis for physicians in diagnosing AD; (iv) positron emission tomography–computed tomography (PET-CT) scans (encompassing Aβ-PET and Tau-PET, voluntary participation), as a diagnostic reference for physicians in diagnosing AD; (v) the analysis of AD blood biomarkers (including Aβ1-40, Aβ1-42, p-Tau, and others, voluntary participation), to further assist physicians in diagnosing AD. On the basis of the data results and following the diagnostic criteria of the National Institute of Neurological and Communicative Disorders and Stroke and the Alzheimer's Disease and Related Disorders Association, the patients are classified as follows:

1) Health ($n = 10$, MoCA ≥ 26 or MMSE ≥ 27);

2) AD ($n = 8$, individuals with abnormalities in the cerebrospinal fluid analysis, PET-CT scans, or blood biomarkers) or probable AD ($n = 1$, CT scan can provide evidence of brain atrophy);

3) MCI ($n = 11$; Because of the absence of results from cerebrospinal fluid analysis, PET-CT scans, or AD blood biomarkers, it is not possible to make a further diagnosis of AD, MoCA = 19 to 25 or MMSE = 21 to 26).

The gender, age, and level of education of the selected participants are presented in table S4. Exclusion criteria for patients in this study include: (i) a history of inflammatory bowel disease, carbohydrate malabsorption, hormonal imbalances, known allergies to food additives, or any other serious medical conditions; (ii) a history of gastrointestinal or cranial surgery; (iii) presence of parasitic infections; (iv) suicidal ideation, self-harm, or aggressive behavior; (v) use of medications known to affect gastrointestinal function, blood pressure, lipid levels, hormone supplements, allergy or asthma medications, proton pump inhibitors, or over-the-counter drugs; (vi) use of probiotics, antibiotics, or prebiotics (dietary fiber and oligosaccharides) in the 8 weeks before the study, alcohol, or drug abuse; (vii) cognitive impairment following various surgeries or a history of significant trauma; (viii) a history of cerebrovascular disease, brain tumors, or cognitive impairment caused by other primary brain lesions. This study has received approval from the Institutional Review Board at Peking University Shenzhen Hospital (research ethics committee of Beijing university Shenzhen hospital, no. 2023-108). All participants must provide written consent before engaging in the study. If a participant is legally incapacitated, then written consent must be obtained from their designated legal custodian.

Animals

All animals were single-housed with a constant temperature of 22° ± 2°C and a relative humidity of 55 ± 5% under a 12/12-hour light-dark cycles (lights on at 8:00 a.m.) in the facility of Northwest A&F University. The animal test protocol follows the guidelines for the care and use of laboratory animals (eighth edition, ISBN-10: 0-309-15, 396-4) and was approved by the Animal Ethics Committee of Northwest A&F University (ethics no. XN2023-0610).

APPswe/PSEN1dE9 (APP/PS1) double-transgenic mice and age-matched WT littermates, on a B6C3-Tg background, were purchased from Model Animal Research Center of Nanjing University (Nanjing, China) and bred in the Northwest A&F University animal facility. APP and Presenilin1 (PSEN1) are regarded as causative genes for AD. The male 5×FAD-transgenic mice (stock no. 006554) on a congenic C57BL6 background were provided by the Jackson Laboratory (Bar Harbor, ME, USA).

IF treatment

Four-month-old WT or APP/PS1 mice (male and female) randomly divided into ad libitum or IF diet groups, including WT + ad libitum (WT mice, $n = 20$), WT + IF (WT mice with IF treatment, $n = 20$), AD + ad libitum (APP/PS1 mice, $n = 20$), and AD + IF (APP/PS1 mice with IF treatment, $n = 20$) for 16 weeks. The IF protocol comprised a day with enough food followed by a day of complete fasting. Food (AIN-93M, TROPHIC Animal Feed Hightech Co. Ltd. Nantong, China) was provided or removed every day at 9:00 a.m., with water supplied ad libitum. Mice were measured for body weight and food intake every 2 days and weekly for water intake.

Antibiotic administration

The set of 4-month-old animals in the validation test were divided into six groups: WT + ad libitum ($n = 5$), WT + ad libitum + ABx ($n = 5$), AD + ad libitum ($n = 4$), AD + ad libitum + ABx ($n = 5$), AD + IF ($n = 5$), and AD + IF + ABx ($n = 4$). The IF regimen was the same as the aforementioned sets. Antibiotic cocktail [penicillin G sodium (1 g/liter), metronidazole (1 g/liter), neomycin sulfate (1 g/liter), streptomycin sulfate (1 g/liter), and vancomycin hydrochloride (0.5 g/liter)] was given in the drinking water starting 14 days before the IF regimen and throughout the experiment.

KCZ (intraperitoneal) injection

A cohort of 10-month-old male APP/PS1 mice underwent stratification into two distinct groups. One of these cohorts underwent intraperitoneal administration of KCZ (MedChemExpress) at a concentration of 1 mg per 1 ml of dimethyl sulfoxide (DMSO) over a 6-week period, equating to 0.05 mg/kg per day ($n = 7$). Concomitantly, the control group of mice received intraperitoneal injections of DMSO ($n = 7$). It is noteworthy that throughout this period, both cohorts of APP/PS1 mice were concurrently subjected to IF treatment.

IPA (gavage) treatment

Five-month-old WT and APP/PS1 mice were administered IPA (Sigma-Aldrich) via gavage at a concentration of 2.5 mg per 1 ml of phosphate-buffered saline (PBS; $n = 6$), corresponding to a dosage of 20 mg/kg per day, over a span of 6 weeks. In parallel, the control group received PBS ($n = 6$).

C. sporogenes and fldC-mutant *C. sporogenes* recolonization

The phenylactyl-CoA dehydratase β-subunit (*fldC*) gene is pivotal for IPA synthesis in *C. sporogenes* ATCC15579 (*C.s.*) (American Type Culture Collection, USA). A *fldC*-mutant *C.s.* (*C.s.* △*fldC*) was obtained from D. Dodd at Stanford University School of Medicine. Both *C.s.* WT and *C.s.* △*fldC* were cultivated under strict anaerobic conditions and suspended in PBS at a concentration of 1×10^{11} colony-forming units (CFU).

For the study, 7-month-old 5×FAD mice underwent a 3-day pretreatment of vancomycin in their drinking water. Subsequently, they were orally gavaged with either *C.s.* WT or *C.s.* △*fldC* strains at a daily dosage of 1×10^{10} CFU for 28 days ($n = 10$ per group) (*22*).

KCZ stereotaxic surgery

Using a stereotactic injection apparatus, KCZ was injected into the hippocampus of 9-month-old 5×FAD mice. The KCZ solution was prepared at 10 mg/ml in DMSO. Injection coordinates were set at medial/lateral (M/L) = 1.2 mm, anterior/posterior (A/P) = −2.0 mm, dorsal/ventral (D/V) = −2.5 mm. Each mouse received a 2-μl dose at a controlled rate of 0.2 μl/min. After the injection, a 10-min wait allowed for KCZ diffusion. The injection site was sealed with sterile bone wax, and the scalp incision was sutured. In the sham surgery group, a 2-μl aliquot of DMSO was injected.

After surgery, each mouse received a 100-μl intraperitoneal injection of ceftriaxone [saline solution (0.5 mg/ml)]. Three days later, the mice were either exposed to a 14-day regimen of IPA treatment or left untreated. IPA was delivered via intraperitoneal injection at a concentration of 2.5 mg/ml in PBS, equivalent to 20 mg/kg per day. In contrast, the control group received PBS injections ($n = 10$ per group).

PXR-shRNA stereotaxic surgery

To further elucidate the role of PXR in IPA-mediated cognitive function in AD mice, we designed an shRNA interference fragment targeting PXR. This PXR-shRNA fragment was constructed into an AAV vector, pAAV-hSyn-EGFP-3xFLAG-WPRE, enabling PXR gene knockdown in neuronal cells, with the target sequence: 5′-CACAACTTTCTCCCACTTCAA-3′. The AAV-expressing PXR-shRNA was injected into the hippocampus of 9-month-old 5×FAD mice via i.c.v. injection. The injection coordinates and postoperative care were consistent with the KCZ (i.c.v.) protocol. Three days postinjection, mice received either IPA or PBS intervention for 14 days (20 mg/kg per day, intraperitoneally) ($n = 8$ per group). Mice were euthanized after 3 weeks of IPA or PBS intervention and behavioral testing following shRNA-PXR (i.c.v.) treatment.

TNFα stereotaxic surgery

After a single intraperitoneal injection of either PBS or IPA (5 or 10 or 20 mg/kg) to 9-month-old C57BL/6J mice for 1 hour, we used cerebral stereotaxy to deliver a one-time TNFα (MedChemExpress) or saline injection directly into the hippocampus. Injection coordinates were precisely set at M/L = 1.2 mm, A/P = −2.0 mm, D/V = −2.5 mm. Each mouse received a 2-μl infusion of TNFα solution (25 mg/ml in saline) at a controlled rate of 0.2 μl/min. Following the injection, a 10-min observation period was observed before needle withdrawal, and the incisions were sutured. After a 4-hour rest, the mice were assessed in the Y-maze.

Biodistribution study of IPA

At 2 months of age, C57BL/6J mice were divided into two groups: one group received intraperitoneal IPA injections (20 mg/kg per day, $n = 16$), and the other group received PBS injections ($n = 16$). Four mice from each group were anesthetized at 0, 1, 2, and 4 hours postinjection. After perfusion with physiological saline, IPA levels in both whole brain and serum were measured ($n = 4$ per group).

Bacterial strains and culture conditions

C.s. WT and *C.s.* △*fldC* were cultivated in GAM medium with a uniform inoculum of 1×10^6 CFU and then cultured at 37°C for 72 hours. IPA was detected in the medium supernatant of *C.s. fldC* by high-performance liquid chromatography (HPLC).

Cell culture

The SH-SY5Y human neuroblastoma cell line was purchased from the National Collection of Authenticated Cell Cultures (Shanghai, China). Cells were maintained in Dulbecco's modified Eagle's medium/F12 medium supplemented with 10% fetal bovine serum, 1% penicillin-streptomycin, and 1% nonessential amino acids (Procell Life Science and Technology Co., China) and cultured at 37°C in a humidified incubator with 5% CO_2.

SH-SY5Y cells were seeded in six-well plates and pretreated with either KCZ (10 μM) or an equivalent volume of DMSO for 1 hour. Subsequently, cells were exposed to IPA (5 μM) or vehicle control. After 6 hours, TNFα (20 ng/ml in PBS) was added to induce an inflammatory response, and incubation continued for an additional 6 hours. Following treatment, cells were harvested for total RNA or protein extraction.

HPLC analysis: Fecal sample extraction

A total of 0.1 g of feces was dissolved in 1 ml of methanol and incubated at 40°C for 20 min with gentle agitation every 5 min. Afterward, the mixture was chilled at −20°C for 20 min and then centrifuged at 12,000 rpm at 4°C for 10 min, and the resulting supernatant was filtered through a 0.22-μm microporous membrane (organic phase).

HPLC analysis: Serum sample extraction

Sixty μl of serum was diluted with prechilled methanol (−20°C) to a total volume of 300 μl. After diluting with methanol, the serum was placed at −20°C for a 20-min incubation period. The samples were then centrifuged and then filtered (as in fecal sample extraction).

HPLC analysis: Brain tissue sample extraction

Within the weighed brain tissue, 500 μl of physiological saline was added and homogenized, and then 10 min of ultrasound was performed. The homogenates were then centrifuged at 4°C and 10,000 rpm for 10 min. Two hundred microliters of the supernatant was mixed with 200 μl of prechilled methanol and subjected it to 5 min of ultrasound. Finally, the samples were centrifuged and filtered, following the same procedure as for fecal sample extraction.

HPLC analysis

The supernatant was filtered and immediately subjected to HPLC (LC-16; Shimadzu, Kyoto, Japan) after centrifugation (14,000*g*, 10 min, 4°C). For IPA analysis, 10 μl of each sample was injected into a chromatograph with a C18 column (Agilent, 4.6 mm by 250 mm, 5 μm) and a fluorescence detector (excitation wavelength/emission wavelength: 282/352 nm) at a column temperature of 30°C. A flow rate of 1.0 ml/min was used with a gradient elution of deionized water (mobile phase A) and 15 mM NAH_2PO_4 (mobile phase B) as follows: 0 to 12 min, 42% A; 12 to 28 min, 50% A; 28 to 35 min, 85% A.

Western blot

Protein expression levels in the hippocampus and SH-SY5Y cells were quantified using the Protein Simple Jess system (Protein Simple, USA). Total tissue proteins were extracted from samples of three mice per group using extraction kits (PL001, ZhongHuiHeCai Biotechnology, China). Protein concentrations were measured with the BCA Protein Assay Kit (A55864, Thermo Fisher Scientific Inc., USA). Protein samples were first prepared by diluting with a sample buffer, followed by mixing with a master mix. The resulting mixture was heated at 95°C for 5 min to achieve complete denaturation. A total of 3 μl of denatured protein, chemiluminescent substrate, primary antibody, and horseradish peroxidase–conjugated secondary antibody were then added to the appropriate wells of the assay plate. A biotinylated protein ladder (12 to 230 kDa) was incorporated into each assay as a molecular weight reference. The plates and capillaries were subsequently placed in the Jess system for automated protein electrophoresis, blocking, antibody incubation, and chemiluminescent signal detection. Data analysis was performed using Compass software (Protein Simple, USA). The following primary antibodies were used for the Western blot analysis: rabbit anti-phospho-NFκB (1:50; Cell Signaling Technology, #3033), rabbit anti-NFκB (1:50; Cell Signaling Technology, #8242), rabbit anti-Mdr1 (1:50; Cell Signaling Technology, #13978), mouse anti-Cyp3a11 (1:50; Abcam, ab22724), rabbit anti–Bace-1 (1:50; Abcam, ab183612), and rabbit anti–glyceraldehyde phosphate dehydrogenase (GAPDH) (1:50; Cell Signaling Technology, #2118).

16*S* rRNA microbiome sequencing

Fecal samples were collected in a clean environment, and total cellular DNA was extracted with the E.Z.N.A. Stool DNA Kit (Omega, Norcross, GA, USA) according to the company's instructions. The bacterial hypervariable V3-V4 region of 16*S* rRNA was chosen for MiSeq (Illumina, CA, USA) paired-end 300-bp amplicon analysis using primers 341_F (5′- CCTACGGGNGGCWGCAG-3′) and 802_R (5′- TACNVGGGTATCTAATCC-3′). Library preparation followed a published method (*9*). The raw reads were merged and trimmed, chimeras were removed, and zero-radius zOTUs with UNOISE was implemented in Search (v2.6.0). The greengenes (13.8) 16*S* rRNA gene database was used as a reference for annotation.

A Kruskal-Wallis test assessed IF's impact on microbial species diversity. Community richness and diversity were evaluated using Chao1, ACE, Shannon, and Simpson indices. Principal coordinate analysis (PCoA) was applied to analyze gut microbiota composition, considering weighted and unweighted UniFrac distances and Bray-Curtis dissimilarity. Permutational multivariate ANOVA (Adonis) with 9999 permutations and analysis of similarities were used to gauge the IF's effect on PCoA β diversity scores. To pinpoint microbial taxa affected by IF, we used PLS-DA within a variable selection (VS) framework, using autoscaled microbiota abundance data. This analysis discriminated AD and WT mouse groups from IF-treated groups (AD + IF and WT + IF), the AD mouse group from the AD + IF group, and the WT mouse group from the WT + IF group, as described in (*58*). We further assessed IF-induced changes in the relative abundance of bacteria selected by VS-PLS-DA using ANOVA, considering sex (females and males) and genotype (APP/PS1 and WT). Significance was determined with a false discovery rate (FDR) threshold of $P < 0.05$. For functional gene predictions, rarified OTU data were used with PICRUSt (v1.1.3). Predicted genes were annotated at various KEGG levels, and significantly enriched pathways were identified using edgeR with an FDR threshold of $P < 0.1$.

Untargeted plasma metabolomics

All samples were analyzed in a single batch using a 1290 Infinity series UHPLC System (Agilent Technologies) with a UPLC BEH Amide column (2.1 mm by 100 mm, 1.7 μm, Waters). The mobile phase consisted of 25 mM ammonium acetate and 25 mM ammonia hydroxide in water (pH 9.75) (A) and acetonitrile (B). The following elution gradient was used: 0 to 0.5 min, 95% B; 0.5 to 7.0 min, 95 to 65% B; 7.0 to 8.0 min, 65 to 40% B; 8.0 to 9.0 min, 40% B; 9.0 to 9.1 min, 40 to 95% B; 9.1 to 12.0 min, 95% B. The column temperature was 25°C, and the autosampler temperature was 4°C, with a 2-μl injection volume. Tandem mass spectrometry (MS/MS) spectra were acquired using the TripleTOF 6600 mass spectrometer (AB Sciex) in an information-dependent manner. The acquisition software, Analyst TF 1.7 (AB Sciex), continuously assessed the full scan survey MS data, triggering the acquisition of MS/MS spectra based on specific criteria. In each cycle, the 12 most intense precursor ions with intensities above 100 were selected for MS/MS analysis at a collision energy of 30 eV, with a cycle time of 0.56 s. Electrospray ionization source conditions included gas 1 at 60 psi, gas 2 at 60 psi, curtain gas at 35 psi, source temperature at 600°C, declustering potential at 60 V, and ion spray voltage floating at 5000 V or −4000 V in positive or negative modes, respectively.

MS raw data (.wiff) files were converted to mzXML using ProteoWizard and processed with XCMS (version 3.2) for peak deconvolution, alignment, and integration. Parameters were set at Minfrac 0.5 and a cutoff of 0.3. An in-house MS/MS database was used for identification. We quantified 1936 and 1887 metabolite features for reverse phase chromatography (RP)+ and RP−, respectively. These were analyzed using VS-PLS-DA and ANOVA to study the IF's impact on the plasma metabolome. Relevant pathways were identified with MetaboAnalyst (*59*).

Integrated multiomics analysis

Multivariate predictive modeling on each omic dataset was conducted using PLS-DA incorporated into a repeated double cross-validations framework (rdCV-PLS-DA). To gain a robust and reliable estimate of model performance, 200 repetitions of the outer cross-validations loop were performed, followed by permutation analysis ($n = 1000$). A multivariate dimension reduction method, DIABLO, was used for multiple omic integration (*60*, *61*). Random use of a full design matrix was used to identify linear combinations of variables from each omic dataset that were maximally correlated. A tuning procedure was used to determine the optimal number of key variables in each dataset to be selected with a minimum misclassification rate. Model performance was then evaluated by 10-fold cross-validation.

RNA sequencing analysis

The total RNA of brain tissue from the hippocampus and SH-SY5Y cells was extracted using TRIzol (Invitrogen, Carlsbad, UA, USA) according to the manufacturer's instructions, followed by being qualified and quantified using a NanoDrop and Agilent 2100 bioanalyzer (Thermo Fisher Scientific, MA, USA). RNA sequencing libraries were prepared using BGISEQ-500 (BGI-Shenzhen, China). Sequencing data were filtered and trimmed using Trimmomatic v0.38 (*62*) to obtain high-quality clean-read data. Clean reads were mapped to the *Mus musculus* genome sequence (http://ftp.ncbi.nlm.nih.gov/genomes/all/GCF/000/001/635/GCF_000001635.26_GRCm38.p6) using Hisat2 v2–2.1.0 (*63*). The reads of each sample were then assembled into transcripts and compared with reference

gene models using StringTie v1.3.4d (*64*). We merged the 55 transcripts to obtain a consensus transcript using a StringTie-Merge program. Transcripts that did not exist in the coding DNA sequence database of the *M. musculus* genome were extracted to predict new genes. The gene expression fragments per kilobase of exon model per million mapped fragments values were calculated using the StringTie Merge program based on the consensus transcript. We then used VS-PLS-DA modeling and ANOVA to identify significant IF-induced changes in gene expression. KEGG and Gene Ontology enrichment analyses were performed using the WebGestalt 2019 (WEB-based Gene Set Analysis Toolkit) (*65*). The most relevant genes associated with IF were further filtered according to KEGG about AD, oxidative phosphorylation, neurotrophin signaling pathway, and synapse (glutamatergic, cholinergic, serotonergic, GABAergic, and dopaminergic). The expression of these genes was subjected to the multiomics analysis integrating with the relative abundance of gut microbiota and plasma levels of metabolites that were affected by IF treatment.

fldC gene detection

Genomic DNA was isolated from mouse colonic contents using the TIANamp Stool DNA Kit (TIANGEN, China) according to the manufacturer's instructions. Reverse transcription qPCR was performed to detect the presence of the *fldC* gene. The primers used for *fldC* amplification were 311F: 5′-TGGGGAATATGATATGTTGTCTGGCATGATG-3′ and 311R: 5′-TGTTCAGCTAATCTATCCATTGGTGTATTCGC-3′ (*44*). The 16*S* rRNA gene was used as an internal reference for normalization.

Statistical analysis

Data were reported as mean ± SEM of at least three independent experiments and analyzed with Tukey's multiple comparisons test by GraphPad Prism 8.0 software (GraphPad Software Inc., San Diego, CA). Two-way ANOVA with Tukey's post hoc test was used to analyze the main IF treatment and the IPA gavage experiments. One-way ANOVA with Tukey's post hoc test was used for the human cohort analysis, antibiotic administration, PXR-shRNA and KCZ (i.c.v.) stereotaxic surgeries, TNFα injection, and all in vitro studies. Unpaired, two-tailed Student's *t* tests were used for the KCZ (intraperitoneal) injection and *C. sporogenes* recolonization experiments. Spearman correlation analysis was used to evaluate the relationship between serum IPA levels and participants' cognitive scores. Statistical significance was presented as mean ± SEM. $*P < 0.05$ and $**P < 0.01$.

Supplementary Materials

The PDF file includes:

Figs. S1 to S10
Tables S4 and S5
Supplementary Methods
Legends for tables S1 to S3
Legends for data S1 and S2
References

Other Supplementary Material for this manuscript includes the following:

Tables S1 to S3
Data S1 and S2

REFERENCES AND NOTES

1. B. D. Arbo, M. F. Ribeiro, L. M. Garcia-Segura, Development of new treatments for Alzheimer's disease based on the modulation of translocator protein (TSPO). *Ageing Res. Rev.* **54**, 100943 (2019).
2. W. A. Eimer, R. Vassar, Neuron loss in the 5XFAD mouse model of Alzheimer's disease correlates with intraneuronal Aβ42 accumulation and Caspase-3 activation. *Mol. Neurodegener.* **8**, 2 (2013).
3. D. K. Kim, D. Han, J. Park, H. Choi, J. C. Park, M. Y. Cha, J. Woo, M. S. Byun, D. Y. Lee, Y. Kim, I. Mook-Jung, Deep proteome profiling of the hippocampus in the 5XFAD mouse model reveals biological process alterations and a novel biomarker of Alzheimer's disease. *Exp. Mol. Med.* **51**, 1–17 (2019).
4. M. V. F. Silva, C. M. G. Loures, L. C. V. Alves, L. C. de Souza, K. B. G. Borges, M. das Graças Carvalho, Alzheimer's disease: Risk factors and potentially protective measures. *J. Biomed. Sci.* **26**, 33 (2019).
5. D. Wahl, V. C. Cogger, S. M. Solon-Biet, R. V. Waern, R. Gokarn, T. Pulpitel, R. de Cabo, M. P. Mattson, D. Raubenheimer, S. J. Simpson, D. G. Le Couteur, Nutritional strategies to optimise cognitive function in the aging brain. *Ageing Res. Rev.* **31**, 80–92 (2016).
6. A. Cherif, B. Roelands, R. Meeusen, K. Chamari, Effects of intermittent fasting, caloric restriction, and ramadan intermittent fasting on cognitive performance at rest and during exercise in adults. *Sports Med.* **46**, 35–47 (2016).
7. T. C. Ooi, A. Meramat, N. F. Rajab, S. Shahar, I. S. Ismail, A. A. Azam, R. Sharif, Intermittent fasting enhanced the cognitive function in older adults with mild cognitive impairment by inducing biochemical and metabolic changes: A 3-year progressive study. *Nutrients* **12**, 2644 (2020).
8. A. R. Vasconcelos, L. M. Yshii, T. A. Viel, H. S. Buck, M. P. Mattson, C. Scavone, E. M. Kawamoto, Intermittent fasting attenuates lipopolysaccharide-induced neuroinflammation and memory impairment. *J. Neuroinflammation* **11**, 85 (2014).
9. Z. Liu, X. Dai, H. Zhang, R. Shi, Y. Hui, X. Jin, W. Zhang, L. Wang, Q. Wang, D. Wang, J. Wang, X. Tan, B. Ren, X. Liu, T. Zhao, J. Wang, J. Pan, T. Yuan, C. Chu, L. Lan, F. Yin, E. Cadenas, L. Shi, S. Zhao, X. Liu, Gut microbiota mediates intermittent-fasting alleviation of diabetes-induced cognitive impairment. *Nat. Commun.* **11**, 855 (2020).
10. Y. Liu, A. Cheng, Y. J. Li, Y. Yang, Y. Kishimoto, S. Zhang, Y. Wang, R. Wan, S. M. Raefsky, D. Lu, T. Saito, T. Saido, J. Zhu, L. J. Wu, M. P. Mattson, SIRT3 mediates hippocampal synaptic adaptations to intermittent fasting and ameliorates deficits in APP mutant mice. *Nat. Commun.* **10**, 1886 (2019).
11. Y. Hu, Y. Yang, M. Zhang, M. Deng, J.-J. Zhang, Intermittent fasting pretreatment prevents cognitive impairment in a aat model of chronic cerebral hypoperfusion. *J. Nutr.* **147**, 1437–1445 (2017).
12. G. P. Dias, T. Murphy, D. Stangl, S. Ahmet, B. Morisse, A. Nix, L. J. Aimone, J. B. Aimone, M. Kuro-O, F. H. Gage, S. Thuret, Intermittent fasting enhances long-term memory consolidation, adult hippocampal neurogenesis, and expression of longevity gene Klotho. *Mol. Psychiatry* **26**, 6365–6379 (2021).
13. J. Zhang, Z. Zhan, X. Li, A. Xing, C. Jiang, Y. Chen, W. Shi, L. An, Intermittent fasting protects against Alzheimer's disease possible through restoring aquaporin-4 polarity. *Front. Mol. Neurosci.* **10**, 395 (2017).
14. B. K. Shin, S. Kang, D. S. Kim, S. Park, Intermittent fasting protects against the deterioration of cognitive function, energy metabolism and dyslipidemia in Alzheimer's disease-induced estrogen deficient rats. *Exp. Biol. Med. (Maywood)* **243**, 334–343 (2018).
15. V. Rajeev, D. Y. Fann, Q. N. Dinh, H. A. Kim, T. M. De Silva, D. G. Jo, G. R. Drummond, C. G. Sobey, M. K. P. Lai, C. L. Chen, T. V. Arumugam, Intermittent fasting attenuates hallmark vascular and neuronal pathologies in a mouse model of vascular cognitive impairment. *Int. J. Biol. Sci.* **18**, 6052–6067 (2022).
16. R. Y. Pan, J. Zhang, J. Wang, Y. Wang, Z. Li, Y. Liao, Y. Liao, C. Zhang, Z. Liu, L. Song, J. Yu, Z. Yuan, Intermittent fasting protects against Alzheimer's disease in mice by altering metabolism through remodeling of the gut microbiota. *Nat. Aging* **2**, 1024–1039 (2022).
17. D. S. Whittaker, L. Akhmetova, D. Carlin, H. Romero, D. K. Welsh, C. S. Colwell, P. Desplats, Circadian modulation by time-restricted feeding rescues brain pathology and improves memory in mouse models of Alzheimer's disease. *Cell Metab.* **35**, 1704–1721.e6 (2023).
18. X. Hu, T. Wang, F. Jin, Alzheimer's disease and gut microbiota. *Sci. China Life Sci.* **59**, 1006–1023 (2016).
19. C. C. Hung, C. C. Chang, C. W. Huang, R. Nouchi, C. H. Cheng, Gut microbiota in patients with Alzheimer's disease spectrum: A systematic review and meta-analysis. *Aging* **14**, 477–496 (2022).
20. X. Guo, X. Zhang, P. Tang, L. Chong, R. Li, Integration of genome-wide association studies (GWAS) and microbiome data highlights the impact of sulfate-reducing bacteria on Alzheimer's disease. *Age Ageing* **52**, afad112 (2023).
21. S. Grabrucker, M. Marizzoni, E. Silajdžić, N. Lopizzo, E. Mombelli, S. Nicolas, S. Dohm-Hansen, C. Scassellati, D. V. Moretti, M. Rosa, K. Hoffmann, J. F. Cryan, O. F. O'Leary, J. A. English, A. Lavelle, C. O'Neill, S. Thuret, A. Cattaneo, Y. M. Nolan, Microbiota from Alzheimer's patients induce deficits in cognition and hippocampal neurogenesis. *Brain* **146**, 4916–4934 (2023).
22. E. Serger, L. Luengo-Gutierrez, J. S. Chadwick, G. Kong, L. Zhou, G. Crawford, M. C. Danzi, A. Myridakis, A. Brandis, A. T. Bello, F. Müller, A. Sanchez-Vassopoulos, F. De Virgiliis, P. Liddell, M. E. Dumas, J. Strid, S. Mani, D. Dodd, S. Di Giovanni, The gut metabolite indole-3 propionate promotes nerve regeneration and repair. *Nature* **607**, 585–592 (2022).

23. Y. J. Chyan, B. Poeggeler, R. A. Omar, D. G. Chain, B. Frangione, J. Ghiso, M. A. Pappolla, Potent neuroprotective properties against the Alzheimer β-amyloid by an endogenous melatonin-related indole structure, indole-3-propionic acid. *J. Biol. Chem.* **274**, 21937–21942 (1999).
24. Q. Zhao, T. Chen, C. Ni, Y. Hu, Y. Nan, W. Lin, Y. Liu, F. Zheng, X. Shi, Z. Lin, J. Zhu, Z. Lin, Indole-3-propionic acid attenuates HI-related blood-brain barrier injury in neonatal rats by modulating the PXR signaling pathway. *ACS Chem. Nerosci.* **13**, 2897–2912 (2022).
25. M. L. Garcez, V. X. Tan, B. Heng, G. J. Guillemin, Sodium butyrate and indole-3-propionic acid prevent the increase of cytokines and kynurenine levels in LPS-induced human primary astrocytes. *Int. J. Tryptophan Res.* **13**, 1178646920978404 (2020).
26. J. Sun, J. Xu, Y. Ling, F. Wang, T. Gong, C. Yang, S. Ye, K. Ye, D. Wei, Z. Song, D. Chen, J. Liu, Fecal microbiota transplantation alleviated Alzheimer's disease-like pathogenesis in APP/PS1 transgenic mice. *Transl. Psychiatry* **9**, 189 (2019).
27. B. J. Moraes, P. Coelho, L. Fão, I. L. Ferreira, A. C. Rego, Modified glutamatergic postsynapse in neurodegenerative disorders. *Neuroscience* **454**, 116–139 (2021).
28. S. M. Dehkordi, M. Arnold, K. Nho, S. Ahmad, W. Jia, G. Xie, G. Louie, A. Kueider-Paisley, M. A. Moseley, J. W. Thompson, L. S. J. Williams, J. D. Tenenbaum, C. Blach, R. Baillie, X. Han, S. Bhattacharyya, J. B. Toledo, S. Schafferer, S. Klein, T. Koal, S. L. Risacher, M. A. Kling, A. Motsinger-Reif, D. M. Rotroff, J. Jack, T. Hankemeier, D. A. Bennett, P. L. De Jager, J. Q. Trojanowski, L. M. Shaw, M. W. Weiner, P. M. Doraiswamy, C. M. van Duijn, A. J. Saykin, G. Kastenmüller, R. Kaddurah-Daouk, Alzheimer's Disease Neuroimaging Initiative and the Alzheimer Disease Metabolomics Consortium, Altered bile acid profile associates with cognitive impairment in Alzheimer's disease-An emerging role for gut microbiome. *Alzheimers Dement.* **15**, 76–92 (2019).
29. D. Dodd, M. H. Spitzer, W. Van Treuren, B. D. Merrill, A. J. Hryckowian, S. K. Higginbottom, A. Le, T. M. Cowan, G. P. Nolan, M. A. Fischbach, J. L. Sonnenburg, A gut bacterial pathway metabolizes aromatic amino acids into nine circulating metabolites. *Nature* **551**, 648–652 (2017).
30. A. Ungurianu, A. Zanfirescu, D. Margină, Sirtuins, resveratrol and the intertwining cellular pathways connecting them. *Ageing Res. Rev.* **88**, 101936 (2023).
31. C. Y. Wang, J. W. Xie, Y. Xu, T. Wang, J. H. Cai, X. Wang, B. L. Zhao, L. An, Z. Y. Wang, Trientine reduces BACE1 activity and mitigates amyloidosis via the AGE/RAGE/NF-κB pathway in a transgenic mouse model of Alzheimer's disease. *Antioxid. Redox Signal.* **19**, 2024–2039 (2013).
32. T. Wang, B. Chen, M. Luo, L. Xie, M. Lu, X. Lu, S. Zhang, L. Wei, X. Zhou, B. Yao, H. Wang, D. Xu, Microbiota-indole 3-propionic acid-brain axis mediates abnormal synaptic pruning of hippocampal microglia and susceptibility to ASD in IUGR offspring. *Microbiome* **11**, 245 (2023).
33. D. Lazic, V. Tesic, M. Jovanovic, M. Brkic, D. Milanovic, B. V. Zlokovic, S. Kanazir, M. Perovic, Every-other-day feeding exacerbates inflammation and neuronal deficits in 5XFAD mouse model of Alzheimer's disease. *Neurobiol. Dis.* **136**, 104745 (2020).
34. Y. Li, J. O. Rinne, L. Mosconi, E. Pirraglia, H. Rusinek, S. DeSanti, N. Kemppainen, K. Någren, B. C. Kim, W. Tsui, M. J. de Leon, Regional analysis of FDG and PIB-PET images in normal aging, mild cognitive impairment, and Alzheimer's disease. *Eur. J. Nucl. Med. Mol. Imaging* **35**, 2169–2181 (2008).
35. T. C. Hammond, X. Xing, C. Wang, D. Ma, K. Nho, P. K. Crane, F. Elahi, D. A. Ziegler, G. Liang, Q. Cheng, L. M. Yanckello, N. Jacobs, A. L. Lin, β-amyloid and tau drive early Alzheimer's disease decline while glucose hypometabolism drives late decline. *Commun. Biol.* **3**, 352 (2020).
36. A. Wani, M. Gupta, M. Ahmad, A. M. Shah, A. U. Ahsan, P. H. Qazi, F. Malik, G. Singh, P. R. Sharma, A. Kaddoumi, S. B. Bharate, R. A. Vishwakarma, A. Kumar, Alborixin clears amyloid-β by inducing autophagy through PTEN-mediated inhibition of the AKT pathway. *Autophagy* **15**, 1810–1828 (2019).
37. A. Virmani, L. Pinto, O. Bauermann, S. Zerelli, Z. Binienda, S. F. Ali, F. R. Leij, Neuronal carnitine palmitoyl transferase1c in the central nervous system: Current visions and perspectives. *J Alzheimers Dis* **4**, 132 (2014).
38. M. Lachén-Montes, A. González-Morales, M. V. Zelaya, E. Pérez-Valderrama, K. Ausín, I. Ferrer, J. Fernández-Irigoyen, E. Santamaría, Olfactory bulb neuroproteomics reveals a chronological perturbation of survival routes and a disruption of prohibitin complex during Alzheimer's disease progression. *Sci. Rep.* **7**, 9115 (2017).
39. C. A. Köhler, M. Maes, A. Slyepchenko, M. Berk, M. Solmi, K. L. Lanctôt, A. F. Carvalho, The gut-brain axis, including the microbiome, leaky gut and bacterial translocation: Mechanisms and pathophysiological role in Alzheimer's disease. *Curr. Pharm. Des.* **22**, 6152–6166 (2016).
40. Y. Xia, Y. Xiao, Z. H. Wang, X. Liu, A. M. Alam, J. P. Haran, B. A. McCormick, X. Shu, X. Wang, K. Ye, *Bacteroides Fragilis* in the gut microbiomes of Alzheimer's disease activates microglia and triggers pathogenesis in neuronal C/EBPβ transgenic mice. *Nat. Commun.* **14**, 5471 (2023).
41. Y. Qiu, Y. Hou, D. Gohel, Y. Zhou, J. Xu, M. Bykova, Y. Yang, J. B. Leverenz, A. A. Pieper, R. Nussinov, J. Z. K. Caldwell, J. M. Brown, F. Cheng, Systematic characterization of multi-omics landscape between gut microbial metabolites and GPCRome in Alzheimer's disease. *Cell Rep.* **43**, 114128 (2024).
42. L. M. Cox, M. J. Schafer, J. Sohn, J. Vincentini, H. L. Weiner, S. D. Ginsberg, M. J. Blaser, Calorie restriction slows age-related microbiota changes in an Alzheimer's disease model in female mice. *Sci. Rep.* **9**, 17904 (2019).
43. F. Pan, L. Zhang, M. Li, Y. Hu, B. Zeng, H. Yuan, L. Zhao, C. Zhang, Predominant gut *Lactobacillus murinus* strain mediates anti-inflammaging effects in calorie-restricted mice. *Microbiome* **6**, 54 (2018).
44. C. Zhang, S. Li, L. Yang, P. Huang, W. Li, S. Wang, G. Zhao, M. Zhang, X. Pang, Z. Yan, Y. Liu, L. Zhao, Structural modulation of gut microbiota in life-long calorie-restricted mice. Structural modulation of gut microbiota in life-long calorie-restricted mice. *Nat. Commun.* **4**, 2163 (2013).
45. W. Zhang, J. Huang, F. Gao, Q. You, L. Ding, J. Gong, M. Zhang, R. Ma, S. Zheng, X. Sun, Y. Zhang, Lactobacillus reuteri normalizes altered fear memory in male Cntnap4 knockout mice. *EBioMedicine* **86**, 104323 (2022).
46. C. Pan, H. Zhang, L. Zhang, L. Chen, L. Xu, N. Xu, X. Liu, Q. Meng, X. Wang, Z.-Y. Zhang, Surgery-induced gut microbial dysbiosis promotes cognitive impairment via regulation of intestinal function and the metabolite palmitic amide. *Microbiome* **11**, 248 (2023).
47. S. Mehrabadi, S. S. Sadr, Assessment of probiotics mixture on memory function, inflammation markers, and oxidative stress in an Alzheimer's disease model of rats. *Iran. Biomed. J.* **24**, 220–228 (2020).
48. T. Ren, Y. Gao, Y. Qiu, S. Jiang, Q. Zhang, J. Zhang, L. Wang, Y. Zhang, L. Wang, K. Nie, Gut microbiota altered in mild cognitive impairment compared with normal cognition in sporadic Parkinson's disease. *Front. Neurol.* **11**, 137 (2020).
49. M. R. Minter, C. Zhang, V. Leone, D. L. Ringus, X. Zhang, P. Oyler-Castrillo, M. W. Musch, F. Liao, J. F. Ward, D. M. Holtzman, E. B. Chang, R. E. Tanzi, S. S. Sisodia, Antibiotic-induced perturbations in gut microbial diversity influences neuro-inflammation and amyloidosis in a murine model of Alzheimer's disease. *Sci. Rep.* **6**, 30028 (2016).
50. C. Wasén, L. C. Beauchamp, J. Vincentini, S. Li, D. S. LeServe, C. Gauthier, J. R. Lopes, T. G. Moreira, M. N. Ekwudo, Z. Yin, P. da Silva, R. K. Krishnan, O. Butovsky, L. M. Cox, H. L. Weiner, Bacteroidota inhibit microglia clearance of amyloid-beta and promote plaque deposition in Alzheimer's disease mouse models. *Nat. Commun.* **15**, 3872 (2024).
51. H. M. Roager, T. R. Licht, Microbial tryptophan catabolites in health and disease. *Nat. Commun.* **9**, 3294 (2018).
52. V. Rothhammer, I. D. Mascanfroni, L. Bunse, M. C. Takenaka, J. E. Kenison, L. Mayo, C. C. Chao, B. Patel, R. Yan, M. Blain, J. I. Alvarez, H. Kébir, N. Anandasabapathy, G. Izquierdo, S. Jung, N. Obholzer, N. Pochet, C. B. Clish, M. Prinz, A. Prat, J. Antel, F. J. Quintana, Type I interferons and microbial metabolites of tryptophan modulate astrocyte activity and central nervous system inflammation via the aryl hydrocarbon receptor. *Nat. Med.* **22**, 586–597 (2016).
53. A. Abildgaard, B. Elfving, M. Hokland, G. Wegener, S. Lund, The microbial metabolite indole-3-propionic acid improves glucose metabolism in rats, but does not affect behaviour. *Arch. Physiol. Biochem.* **124**, 306–312 (2018).
54. C. S. Kim, S. Jung, G. S. Hwang, D. M. Shin, Gut microbiota indole-3-propionic acid mediates neuroprotective effect of probiotic consumption in healthy elderly: A randomized, double-blind, placebo-controlled, multicenter trial and in vitro study. *Clin. Nutr.* **42**, 1025–1033 (2023).
55. C. H. Chen, W. Zhou, S. Liu, Y. Deng, F. Cai, M. Tone, Y. Tone, Y. Tong, W. Song, Increased NF-κB signalling up-regulates BACE1 expression and its therapeutic potential in Alzheimer's disease. *Int. J. Neuropsychopharmacol.* **15**, 77–90 (2012).
56. X. Zhang, Q. Zou, B. Zhao, J. Zhang, W. Zhao, Y. Li, R. Liu, X. Liu, Z. Liu, Effects of alternate-day fasting, time-restricted fasting and intermittent energy restriction DSS-induced on colitis and behavioral disorders. *Redox Biol.* **32**, 101535 (2020).
57. L. K. Heilbronn, S. R. Smith, C. K. Martin, S. D. Anton, E. Ravussin, Alternate-day fasting in nonobese subjects: Effects on body weight, body composition, and energy metabolism. *Am. J. Clin. Nutr.* **81**, 69–73 (2005).
58. L. Shi, J. A. Westerhuis, J. Rosén, R. Landberg, C. Brunius, Variable selection and validation in multivariate modelling. *Bioinformatics* **35**, 972–980 (2019).
59. Z. Pang, J. Chong, S. Li, J. Xia, MetaboAnalystR 3.0: Toward an optimized workflow for global metabolomics. *Metabolites* **10**, 186 (2020).
60. A. Singh, C. P. Shannon, B. Gautier, F. Rohart, M. Vacher, S. J. Tebbutt, K. A. Lê Cao, DIABLO: An integrative approach for identifying key molecular drivers from multi-omics assays. *Bioinformatics* **35**, 3055–3062 (2019).
61. F. Rohart, B. Gautier, A. Singh, K. A. Lê Cao, mixOmics: An R package for 'omics feature selection and multiple data integration. *PLOS Comput. Biol.* **13**, e1005752 (2017).
62. A. M. Bolger, M. Lohse, B. Usadel, Trimmomatic: A flexible trimmer for Illumina sequence data. *Bioinformatics* **30**, 2114–2120 (2014).
63. D. Kim, B. Langmead, S. L. Salzberg, HISAT: A fast spliced aligner with low memory requirements. *Nat. Methods* **12**, 357–360 (2015).
64. M. Pertea, G. M. Pertea, C. M. Antonescu, T. C. Chang, J. T. Mendell, S. L. Salzberg, StringTie enables improved reconstruction of a transcriptome from RNA-seq reads. *Nat. Biotechnol.* **33**, 290–295 (2015).
65. Y. Liao, J. Wang, E. J. Jaehnig, Z. Shi, B. Zhang, WebGestalt 2019: Gene set analysis toolkit with revamped UIs and APIs. *Nucleic Acids Res.* **47**, W199–W205 (2019).

66. L. M. Lueptow, Novel object recognition test for the investigation of learning and memory in mice. *J. Vis. Exp.* , e55718 (2017).
67. Y. Zhao, Q. Wang, M. Jia, S. Fu, J. Pan, C. Chu, X. Liu, X. Liu, Z. Liu, (+)-Sesamin attenuates chronic unpredictable mild stress-induced depressive-like behaviors and memory deficits via suppression of neuroinflammation. *J. Nutr. Biochem.* **64**, 61–71 (2019).
68. Q. Wang, M. Jia, Y. Zhao, Y. Hui, J. Pan, H. Yu, S. Yan, X. Dai, X. Liu, Z. Liu, Supplementation of sesamin alleviates stress-induced behavioral and psychological disorders via reshaping the gut microbiota structure. *J. Agric. Food Chem.* **67**, 12441–12451 (2019).

Acknowledgments: We thank D. Dodd and Y. Liu from Stanford University for providing the mutant *C. sporogenes* strain. We appreciate the support from the platform of Northwest A&F University Gene Editing Scientific Teaching (NWAFU-GEST). We also thank Y. Zhou and Q. Zhang from the instruments shared platform of the College of Food Science and Engineering and Life Science Research Core Services of NWAFU, for the assistance of instruments and facility. **Funding:** This work was financially supported by the National Science and Technology Innovation 2030-Major Program of Brain Science and Brain-Like Research (no. 2022ZD0208100, Z.L.), the National Natural Science Foundation of China (no. 3224100327, Z.L.), and Shenzhen Science and Technology Program (no. JCYJ20220818102810022, J.H.). **Author contributions:** L.L., M.J., C.Y., Y.Z., J.H., Y.Z., X.H., F.N., C.D., Q.L., J.G., X.J., K.X., Y.W., L.D., S.Z., and L.S. performed the experiments and analyzed the data; Z.L., X.L., and X.C. designed the study; Z.L., L.S., Y.Z., M.J., and L.L. wrote the paper. M.J., L.S., and L.L. prepared the figures. All authors discussed the results and commented on the paper. **Competing interests:** The authors declare that they have no competing interests. **Data and materials availability:** The raw and processed data of RNA sequencing in the current study were deposited on GEO (https://ncbi.nlm.nih.gov/geo/query/acc.cgi?acc=GSE164461), and the sequencing data have been deposited in the NCBI database under accession number GSE164461.

Submitted 18 February 2025
Accepted 31 October 2025
Published 28 November 2025
10.1126/sciadv.adw8410